Metabolic and Population Profiles of Active Subseafloor Autotrophs in Young Oceanic Crust at Deep-Sea Hydrothermal Vents

Sabrina M. Elkassas,[a,b,#] Caroline S. Fortunato,[c,d] Sharon L. Grim,[a] David A. Butterfield,[e] James F. Holden,[f] Joseph J. Vallino,[c] Christopher K. Algar,[g] Lisa Zeigler Allen,[h,i] Benjamin T. Larson,[e] Giora Proskurowski,[e,j] Emily Reddington,[c,k] Lucy C. Stewart,[f,l] Begum Topçuoğlu,[f,m] and Julie A. Huber[a,#]

[a]Department of Marine Chemistry and Geochemistry, Woods Hole Oceanographic Institution, Woods Hole, MA, USA

[b]Department of Earth, Atmospheric, and Planetary Sciences, Massachusetts Institute of Technology, Cambridge, MA, USA

[c]Ecosystems Center, Marine Biological Laboratory, Woods Hole, MA, USA

[d]Present address: Department of Biology, Widener University, Chester, PA, USA

[e]Cooperative Institute for Climate, Ocean & Ecosystem Studies, University of Washington, Seattle, WA, USA

[f]Department of Microbiology, University of Massachusetts Amherst, Amherst, MA, USA

[g]Department of Oceanography, Dalhousie University, Halifax, Nova Scotia, Canada

[h]Scripps Institution of Oceanography, University of California, San Diego, La Jolla, CA, USA

[i]Department of Microbial and Environmental Genomics, J. Craig Venter Institute, La Jolla, CA, USA.

[j]Present address: MarqMetrix, ThermoFisher Scientific, Seattle, WA

[k]Present address: Great Pond Foundation, Edgartown, MA, USA

[l]Present address: New Zealand Association of Scientists, Wellington, NZ

[m]Present address: Bristol Myers Squibb, Summit, NJ, USA

Running Head: RNA-SIP of microbial autotrophs at hydrothermal vents

[#]Address correspondence to Sabrina Elkassas, elks@mit.edu and Julie Huber, jhuber@whoi.edu

Sabrina Elkassas and Caroline Fortunato contributed equally to this work. Julie Huber, the final author listed, is the Principal Investigator on this project.

ABSTRACT

At deep-sea hydrothermal vents, magmatically driven rock-water reactions in the crust generate gases and other reduced compounds that subseafloor microorganisms use for chemolithoautotrophy. In this study, microbial autotrophs from three diffuse flow hydrothermal vents at Axial Seamount in 2013 and 2014 were isotopically labeled using RNA Stable Isotope Probing (RNA-SIP), targeting subseafloor autotrophic mesophiles (30°C), thermophiles (55°C), and hyperthermophiles (80°C). We constructed taxonomic and functional profiles of active chemolithoautotrophs, examined population distributions across sites, and linked primary producers to their specific metabolic strategies within the subseafloor community. Dominant autotrophs exhibited hydrogen-dependent dissimilatory metabolisms such as sulfur and nitrate reduction and methanogenesis, as well as microaerophilic sulfide oxidation even at 80°C, consistent with fluid chemistries at each site. While hydrogenotrophic methanogenic archaea such as *Methanothermococcus* were restricted in their distribution and activity, hydrogenotrophic sulfur and nitrate reducers from the Aquificota (*Thermovibrio*), Campylobacterota (Nautiliaceae, *Hydrogenimonas*, and Desulfurobacteriaceae) were consistently active and present at all sites and years at both the population and community levels. Hydrogenase transcripts were significantly differentially expressed, and diverse hydrogenases were found in metagenome-assembled genomes of Aquificota members, highlighting the importance and versatility of their hydrogen utilization strategies which likely contribute to their cosmopolitan distribution across

geochemically disparate subseafloor sites. Together, this study provides new insights into the functional dynamics and distribution of key subseafloor autotrophic microbial communities in young oceanic crust at deep-sea hydrothermal vents.

Keywords: deep-sea hydrothermal vents, RNA-SIP, chemolithoautotrophy, diffuse flow

IMPORTANCE

Deep-sea hydrothermal vents are hotspots for life in the dark ocean, where rich animal ecosystems are supported by microbial primary producers utilizing the abundant chemical energy supplied by high-temperature water-rock reactions. Despite increasing knowledge about the geochemistry and microbiology of deep-sea hydrothermal vents, there is still a gap in our understanding of the key microbial players who fix much of the carbon at these sites, especially in the productive subseafloor. In this study, stable isotope probing was used to label active microbial autotrophs in diffuse flow venting fluids from three sites over two years and was combined with metatranscriptomic sequencing to identify their specific metabolic strategies. This research highlights the microbial community composition, function, gene regulation, and population dynamics that enable hydrothermal ecosystems to persist.

INTRODUCTION

Deep-sea hydrothermal systems span large temperature and geochemical gradients, from cold, oxidized seawater to hot, highly reduced hydrothermal fluid produced by rock-water reactions. There is a wide diversity of microbial niches at deep-sea hydrothermal vents, many of which are powered by chemolithoautotrophy, including chimneys, animals, venting fluids, hydrothermal plumes, mats, and the subseafloor (1). Mixing zones at and below the seafloor can be sampled through diffuse flow vents (~5-120°C), providing a glimpse into the subseafloor

habitat within oceanic crust, one of the most productive microbial niches in the vent environment (2-11).

Phylogenetic, metagenomic, and metatranscriptomic studies of diffuse flow microbial communities have expanded our knowledge on the composition and variability of these communities over time and space, considering tectonic setting, host rock type, and geochemistry (e.g. 1, 7-10, 12-22). Many of the studies of diffuse flow microbial communities occurred at Axial Seamount, an active deep-sea volcano on the Juan de Fuca Ridge in the northeast Pacific Ocean where there is a long history of coupled microbiological and geochemical research (6, 8, 12, 18). Venting fluids at Axial host a diverse community of microorganisms composed of Campylobacterota, Aquificota, and methanogenic archaea carrying out sulfide and hydrogen oxidation, sulfur and nitrate reduction, and methanogenesis (8, 10, 12, 15, 17, 22). The diffuse flow microbial communities identified in these studies include a mix of seawater, seafloor, and subseafloor populations that inhabit a wide range of temperatures along diverse geochemical gradients, making it difficult to pinpoint which microbes are active in the subseafloor, especially in the warmer, deeper portions of the subseafloor. However, the recent application of stable isotope probing (SIP) is providing new insights into microbial activity in the dynamic and hard-to-access subseafloor environment (8, 11, 23-24), including RNA Stable Isotope Probing (RNA-SIP).

RNA-SIP is an experimental technique by which isotopically labeled substrate is added to environmental samples at near-natural conditions, incubated, and the label incorporation is probed at the genetic level through sequencing of transcripts (8, 25-26). Resulting isotope-enriched RNA-SIP metatranscriptomes reveal the identity and functional attributes of the microbes that incorporate the labeled substrates in each community under defined experimental conditions (8, 25-26). The first application of this method to deep-sea ecosystems was at Axial Seamount, where

92 in 2013, Marker 113 diffuse fluid was incubated with labeled bicarbonate to target autotrophs at
93 mesophilic, thermophilic, and hyperthermophilic temperature regimes in the subseafloor (8).
94 Results revealed shifts in dominant taxa, metabolisms, and carbon fixation pathways across the
95 temperature spectrum when compared to the unmanipulated fluid. The method was later used at
96 multiple hydrothermal vent sites along the Mariana back-arc, where thermophilic RNA-SIP
97 incubations found that Campylobacterota were active and present at all but one sampled vent,
98 which had a high abundance and activity of Aquificota. These differences were attributed to
99 variation in hydrothermal activity due to underlying tectonic setting (23). This method was also
100 carried out *in situ* at Axial using a novel instrument to complete the RNA-SIP experiment on the
101 seafloor. Comparison of shipboard and seafloor incubations at 55°C found that thermophilic,
102 autotrophic Campylobacterota that oxidized hydrogen coupled with nitrate reduction were
103 dominant in all experiments, but transcripts for thermal stress proteins were significantly more
104 abundant in the shipboard experiments (24). While ideally, all manipulative experiments like
105 RNA-SIP would be conducted without sample lag time and depressurization to alleviate stress and
106 the disappearance of certain electron acceptors like oxygen and methane, the dominant microbes
107 and metabolisms in all experiments were nearly identical.

108 Building on a legacy of microbiological and geochemical studies at Axial Seamount and
109 hydrothermal systems elsewhere, we expand on these studies to include two years of RNA-SIP
110 data from three diffuse flow vent sites at three temperatures to examine how the dominant
111 microbial subseafloor autotrophs at Axial Seamount vary with temperature, fluid chemistry,
112 geology of the vent (sulfide vs. basalt), space, and time. This study contributes new *in situ* oxygen
113 data as well as an expansive metatranscriptomic dataset that enabled differential expression
114 analysis of transcripts across temperatures within and among vents, and between years. We

determined the specific geochemical and thermal conditions under which autotrophic communities and populations are active and identified potential competition amongst these microbial groups for electron acceptors and donors, including oxygen, nitrate, and hydrogen. Overall, these findings expand our knowledge of the distribution and energy acquisition strategies of active microbial assemblages in the productive deep-sea hydrothermal vent subseafloor at a mid-ocean ridge spreading center.

RESULTS

Marker 113, Anemone, and Marker 33 were chosen for sampling in this comparative study because they are situated among three different vent fields within the Axial caldera, and are geochemically and microbiologically distinct (10, 27-28; Fig S1). Chemical characteristics of all diffuse flow vents are shown in Table 1 and Table S1 and include data from both previously published work as well as new oxygen data collected with an *in situ* probe (10, 28; Figs 1 and 2, Table S2).

Marker 113 vent is located on top of a lava pillar at the edge of a collapse zone within an inflated lobate basalt flow. Marker 33 is located near the eruptive fissures that fed the 1998 and 2011 eruptions, both of which covered the Marker 33 vent site. There are no high-temperature vents directly adjacent to Marker 113 or Marker 33. The nearest high-temperature vents are in the International District vent field located 0.6 km northeast of Marker 113 and 0.8 km south of Marker 33. Previous work (28) estimated the end-member hydrogen and methane concentrations feeding Marker 113 and Marker 33 vents using extrapolated chloride end-members for those two vents and the average high-temperature fluid compositions for those chloride concentrations (Table S1, Fig S2). In contrast, Anemone vent is part of a flat, actively growing sulfide mound fed by a high-temperature source fluid that diffuses through sulfide minerals and exits through very small, hot

vent orifices with weak flow, with end-member fluid within a meter of the diffuse flow site sampled. At all three locations, the high-temperature source fluid can be compared with the paired diffuse flow fluid samples to infer changes in chemistry that occur in the shallow subseafloor within the basalt and/or sulfide mineral matrix.

At all diffuse flow vents, the temperatures ranged from 18.5-28.2°C during sampling, the pH was on average ~5.6, and the microbial cell concentrations were the same order of magnitude at each site (1.7-6.8 x 10^5 cells/mL) and all an order of magnitude above concentrations in background seawater (Table 1). However, there were clear differences in the diffuse fluid chemical composition among the three vents in this study (Figs 1 and 2, Tables 1, S1, and S2). All of the venting sites were depleted in oxygen relative to near-bottom seawater in the Axial caldera (31 µmol/kg, +/- 2µmol/kg, n=24), and a linear regression of the recorded sample temperature and *in situ* oxygen concentration indicated oxygen behaves differently at each site, with zero oxygen predicted to occur at 33°C for Marker 113 and at 52°C for Marker 33, while oxygen data from Anemone points to zero oxygen at temperatures greater than 100°C (Fig 1). Additional biologically relevant chemical constituents for the diffuse fluid vents and their closest high-temperature end-member were plotted against Mg to examine deviations from conservative mixing as potential evidence of microbial activity in the venting fluids (Fig 2). At Marker 113 and 33, NO_3^- (Fig 2A) and H_2 (Fig 2B) were depleted, and CH_4 concentrations were elevated (Fig 2C). At Anemone, there was evidence for depletion of H_2 (Fig 2B). Anemone also had the highest H_2S concentrations in both years compared to the other two sites (Table 1).

	Seawater	Anemone subseafloor source	Anemone diffuse vent	Anemone diffuse vent	Marker 33 subseafloor estimated source	Marker 33 diffuse vent	Marker 33 diffuse vent	Marker 113 subseafloor estimated source	Marker 113 diffuse vent	Marker 113 diffuse vent
Year	2015		2013	2014		2013	2014		2013	2014
Depth (m)	1520	1542.8	1542	1539		1516	1514		1520	1518
Temperature (°C)	2	232.4	28.2	20.3	340	27.3	18.5	340	24.5	24.3
pH	7.8	4.3	5.5	5.1	4	5.5	5.6	3.3	6.2	5.8
NO_3^- (μmol/kg)	39	0	35.5	35.2	0	18.3	28.2	0	7.2	8.1
H_2 (μmol/kg)	0.002	360	13.9	27.7	300	1.5	1.5	950	1.4	1
H_2S (μmol/kg)	0	7400	1036	964.7	n.d.	545	262	n.d.	729	556
CH_4 (μmol/kg)	0.002	205	14.8	31.7	70	19	6.4	56	16.9	38
Mg (mmol/kg)	52.4	0	46.5	45.6	0	45.9	48.1	0	50.2	48.8
O_2 (μmol/L)	31	0	14.4	17.6	0	14.7	23.3	0	7	9.9
Cl^- (μmol/L)	541	315	513	518	390	520	526	100	521	518
Percent Seawater	100	3.3	88.9	87	0	87.7	91.9	0	96	96.4
Microbial cells mL^{-1}	2.4×10^6		4.1×10^5	1.7×10^5		4.2×10^5	3.9×10^5		4.6×10^5	6.8×10^5

n.d. = no data

Table 1. Measurements of chemical species and microbial counts for diffuse vent sites Anemone, Marker 33, and Marker 113 from 2013 and 2014 as reported in Fortunato *et al*. 2018 (10), as well as the nearby high temperature end-member chemistry. H_2 and CH_4 for Marker 33 and 113 end-members were estimated using methods described in Stewart *et al*., 2019 (28). Percent seawater was extrapolated using magnesium as a conservative tracer: [Mg]vent/[Mg]seawater × 100, and background seawater Mg concentration at 1500 m was 52.4 mmol/kg.

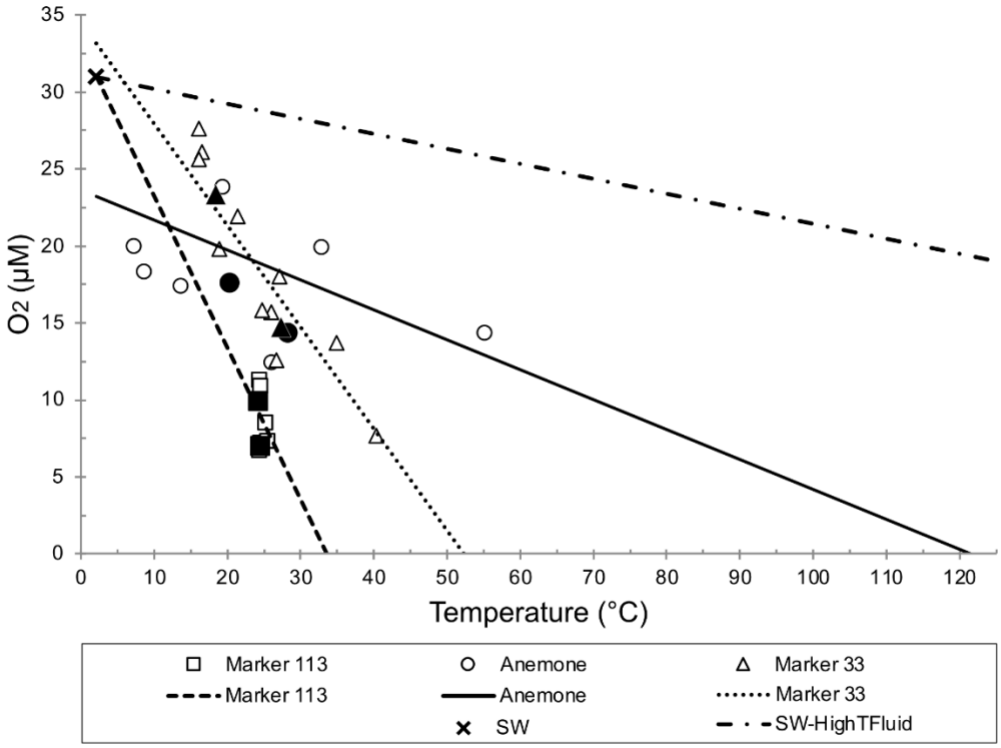

Figure 1. *In situ* oxygen versus temperature for diffuse vents sampled for this study. Near-bottom seawater averages 31 µmol/kg (+/- 2.2). Linear regression lines are drawn for each of the three vent sites for the two years sampled, including the ambient seawater point in the regression. The SW-HighTFluid line is between seawater and a hypothetical zero-oxygen end-member at 325°C. Solid data points indicate the exact fluid sampling bag used in the SIP experiment.

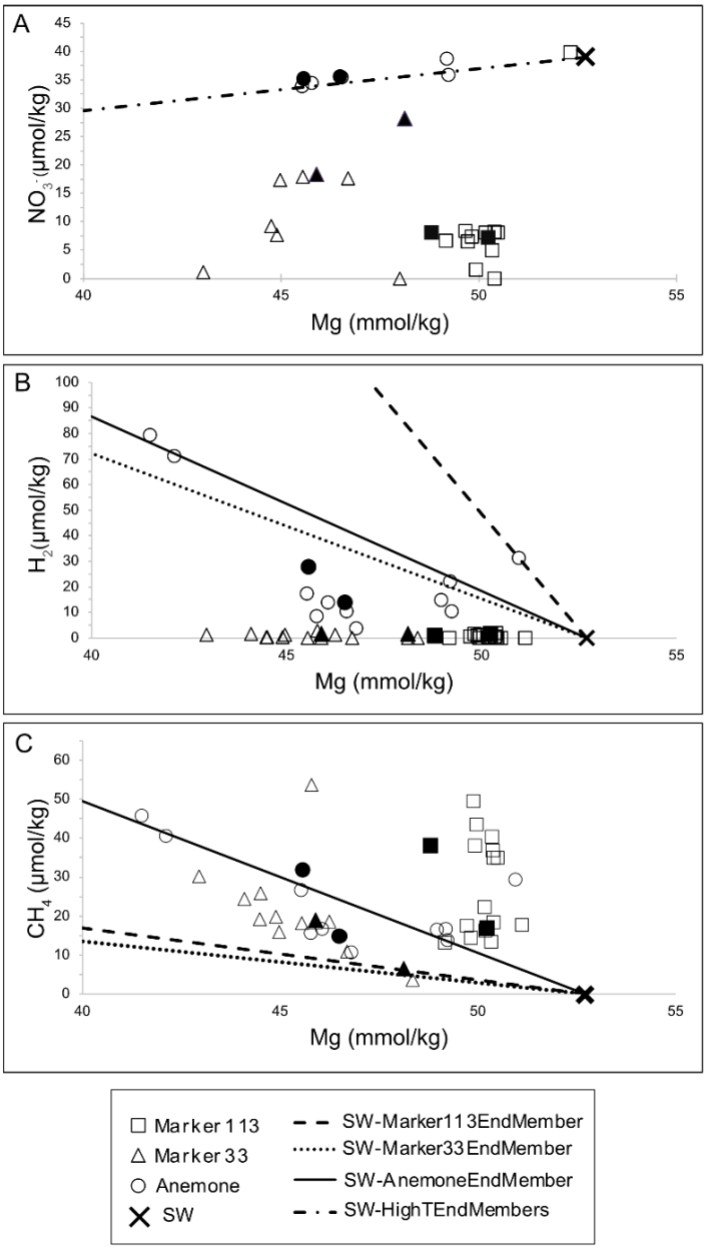

Figure 2. Vent chemical species measured at diffuse vent sites Marker 113, Anemone, and Marker 33 in 2013 and 2014. Regression lines are drawn from seawater to end-member fluid concentration for each vent and chemical species to represent conservative mixing between seawater and the high-temperature fluid for **A.** NO_3^-. All vent end-members had 0 NO_3^-, so the single regression line is between a 0 Mg/0 NO_3^- end-member and seawater. **B.** H_2 and **C.** CH_4 concentrations. Solid data points indicate the exact fluid sampling bag used in the SIP experiment.

179 *RNA-SIP experiments*

180 In total, 15 sets of RNA stable isotope probing experiments were carried out in 2013 and 2014
181 using fluids collected from Marker 113, Anemone, and Marker 33 (Tables 2, S3, and S4). All 15
182 RNA-SIP experiments showed a heavier buoyant density peak of RNA in the ^{13}C-labeled
183 experiment compared to the ^{12}C-labeled control, indicating uptake of labeled bicarbonate into
184 RNA (Figs S3-S5). The highest RNA concentration was chosen from the ^{12}C-light and ^{13}C-heavy
185 peaks for sequencing. If the experiment had two RNA peaks, the two peak fractions were pooled
186 together and sequenced as one sample (Marker 113 at 30 and 80°C, Fig S3C and S5C). For
187 experiments that had two time points, the ^{12}C-light and ^{13}C-heavy peaks from both time points
188 were sequenced. Corresponding ^{13}C-light and ^{12}C-heavy fractions were also sequenced as
189 additional controls, but given their very low RNA concentrations, the sequencing results were not
190 always successful, and these data were not included in any subsequent analyses.

191 Including technical sequencing replicates, there were 84 total metatranscriptomes (44 ^{13}C-
192 heavy and ^{12}C-light, 34 ^{13}C-light and ^{12}C-heavy RNA-SIP experimental metatranscriptomes, and
193 six metatranscriptomes from the *in situ* unmanipulated vent fluid; Table S3) included in this study,
194 totaling over a billion high-quality reads from paired-end Illumina sequencing. Real-time
195 quantitative Reverse Transcription Polymerase Chain Reaction (qRT-PCR) was subsequently
196 carried out to normalize data across experiments using 16S rRNA copies, as shown in Figures S3-
197 S5 (29, 30). In most cases, the highest concentration of RNA corresponded to the highest rRNA
198 copy number.

199 Results from the ^{13}C-heavy RNA-SIP metatranscriptomes are presented as ^{13}C-enriched
200 transcripts throughout the manuscript to distinguish these results from the metatranscriptomes of
201 unmanipulated diffuse fluids. As described in the Methods and Supplementary Methods, the ^{13}C-

202 enriched fraction of the RNA-SIP metatranscriptomes were annotated and compared with the
203 paired metagenome and metatranscriptome generated from unmanipulated diffuse fluids that were
204 filtered and fixed on the seafloor. This comparison enabled both annotation and interpretation of
205 experimental results and ensured results were representative of the native hydrothermal vent
206 microbial community. We used multiple bioinformatic tools to examine this complex ^{13}C-enriched
207 RNA-SIP metatranscriptomic dataset, including transcript taxonomy to provide detailed microbial
208 community composition profiles (Fig 3) for each experiment, as well as experiment-derived MAG
209 read recruitment to determine specific population distributions (Fig 4). We also analyzed
210 taxonomy and activity of metabolism-specific genes (Fig 5), coupled with a functional-agnostic
211 approach with multiple differential gene expression analyses (Fig 6).
212
213 **Table 2**. RNA-SIP experiments conducted, showing vent name, year, temperature of experiment, and time
214 points collected during incubation.

Vent	**Year**	**30 °C**	**55 °C**	**80 °C**
Marker 113	2013	36 hr	36 hr	18 hr*
Marker 113	2014	n.d.	18 hr, 36 hr	9 hr
Anemone	2013	n.d.	n.d.	18 hr*
Anemone	2014	24 hr, 36 hr	18 hr, 36 hr	18 hr
Marker 33	2013	36 hr	36 hr	36 hr
Marker 33	2014	24 hr, 36 hr	18 hr, 36 hr	9 hr, 18 hr

n.d. = no data; * = 1 L LVWS sample

215 *Taxonomic composition of unmanipulated fluids and ^{13}C-enriched fraction of RNA-SIP*
216 *experiment microbial communities*

217 The unmanipulated fluid metatranscriptomes represent the taxa with detectable transcripts at
218 the instant of sampling via filtration and immediate RNALater fixation on the seafloor. The
219 taxonomy of *in situ* active microbial community members as well as those in the ^{13}C-enriched
220 fraction of RNA-SIP experiments was acquired by mapping non-rRNA transcripts to
221 taxonomically classified metagenomic contigs and then normalizing the genera in each sample to
222 100% (Fig 3A-D). The taxonomy of the unmanipulated fluids was compared to both the ^{12}C-light
223 and ^{13}C-enriched RNA-SIP taxonomy (Fig S6). In all but one experiment, the taxonomy of the
224 ^{12}C-light RNA-SIP metatranscriptomes was similar to the ^{13}C-enriched fraction and therefore
225 results here and throughout will focus only on the ^{13}C-enriched fraction metatranscriptomes, as
226 they represent the population of isotope-enriched (active) microbes (Fig 3).

227 All genera active at 30°C in the ^{13}C-enriched RNA-SIP metatranscriptomes were also
228 identified in the unmanipulated fluid metatranscriptomes (Fig 3A). When comparing across all
229 three sites at 30°C, most of the active community was comprised of members of the
230 Campylobacterota. *Sulfurimonas* transcripts were observed at all three vents but were most
231 abundant at Marker 113 (52%) and Marker 33 (31.3%) (Fig 3B). Transcripts of *Cetia* (16.8-33.2%)
232 and *Caminibacter* (12.5-22.2%) were found only in the ^{13}C-enriched fraction of RNA-SIP
233 experiments from Anemone. At Marker 33, transcripts belonging to *Hydrogenimonas* (34.3%)
234 were more abundant compared to the other vents.

235 Like the 30°C experiments, all genera active at 55°C in the ^{13}C-enriched fraction of the
236 RNA-SIP metatranscriptomes were also identified in the unmanipulated fluid metatranscriptomes
237 (Fig 3A). Across all three sites at 55°C, the major differences in taxonomy compared to the 30°C

238 ^{13}C-enriched fraction of the RNA-SIP experiments were a shift to higher relative abundance of
239 *Cetia, Caminibacter, Nautilia,* and *Hydrogenimonas* transcripts, rather than *Sufurimonas*
240 transcripts (Fig 3C). Transcripts from *Caminibacter, Cetia, Nautilia*, and *Hydrogenimonas*
241 dominated in experiments from Marker 113 and Marker 33, but in 2013, these experiments also
242 had transcripts for thermophilic methanogens. *Methanothermococcus* comprised 17.3% and 18.6%
243 of the 2013 ^{13}C-enriched fraction of community transcripts at Marker 113 and Marker 33,
244 respectively, and were completely absent at Anemone in 2014, where both timepoints of 55°C
245 experiments were like those at 30°C, except for the absence of *Sulfurimonas* (Fig 3C). Further, the
246 ^{13}C-enriched population at Anemone in 2014 had the same Campylobacterota taxa as seen at
247 Marker 113 and 33 at 55°C.

248 Unlike at 30°C and 55°C, where Campylobacterota were abundant in both SIP experiments
249 and unmanipulated fluids, many ^{13}C-enriched active taxa at 80°C were in low abundance in the
250 unmanipulated fluids (Fig. 3A), including those from Phylum Aquificota and *Methanotorris* at
251 Marker 113, *Phorcysia* at Anemone, and *Thermovibrio* at Marker 33. The major differences in
252 taxonomy in the ^{13}C-enriched fraction of 80°C RNA-SIP metatransciptomes across sites included
253 a higher abundance of methanogenic groups at Marker 113 and 33, the presence of *Aquifex* only
254 at Anemone, and persistent detection of *Desulfurobacterium* and *Thermovibrio* at all sites and
255 years. In the Marker 113 experiments at 80°C in 2013 (Fig 3D), close to half of all transcripts were
256 from hyperthermophilic methanogens, including *Methanocaldococcus* (37.6%) and *Methanotorris*
257 (2.5%). Methanogenic groups were not detected in the ^{13}C-enriched fraction in 2014 at Marker
258 113. Hyperthermophilic methanogens were observed at Marker 33 in the ^{13}C-enriched fraction in
259 2014, along with a large proportion of transcripts classified to Aquificota, including the genera

260 *Phorcysia, Thermovibrio,* and *Desulfurobacterium*. Transcripts for these genera were also

261 abundant at Marker 113 in 2014, when methanogen transcripts were absent (Fig 3D).

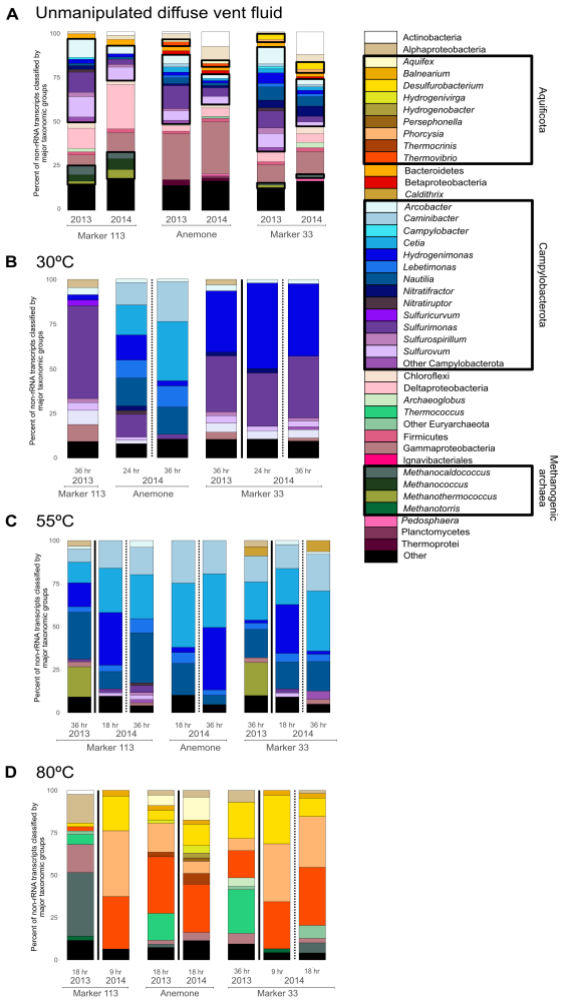

262

263 **Figure 3.** Relative abundance of major taxonomic groups of **A**. Annotated non-rRNA transcripts from

264 unmanipulated fluid metatranscriptomes and annotated non-rRNA transcripts from the ^{13}C-enriched

265 fraction of RNA-SIP experiments at **B**. 30°C, **C**. 55°C, and **D**. 80°C. Black boxes indicate the main

266 autotrophic taxonomic groups recovered from the ^{13}C-enriched fraction of RNA-SIP metatranscriptomes

267 and are drawn onto **3A** to show how these taxa make up a small proportion of the overall unmanipulated

268 fluid metatranscriptome to then become the key autotrophs in the ^{13}C-enriched fraction of RNA-SIP

269 metatranscriptomes in **3B-D.**

Metagenome assembled genomes (MAGs)

Binning of the co-assembly of all unmanipulated diffuse fluid, background, and plume metagenomes from Fortunato *et al*., (2018) resulted in 391 MAGs, with 120 bins remaining after filtering for quality (completeness ≥70%, contamination ≤10% based on the presence of single copy bacterial and archaeal marker genes) (10, Table S5). For a phylogenetic tree of the 120 quality-filtered bins, see Figure S7. These bins were further filtered to remove known heterotrophs and representatives solely sourced from the plume, background, or 2015 metagenomes, resulting in 25 bins. The final 11 MAGs from genomic binning from all diffuse fluid metagenomes were selected based on having >4% of their coding genome expressed [length of expressed genes(bp)/genome length (bp)] in any individual RNA-SIP ^{13}C-enriched fraction (Fig 4, Tables S5 and S6). The taxonomy of the highly transcribed MAGs was comparable to the ORF transcript taxonomy assignments (Figs 3, 4), including groups primarily from the Aquificota, Campylobacterota, and methanogens.

Both Marker 113 and Marker 33 had *Sulfurimonas* populations (bin 41) transcribed at 30°C (Fig 4), corresponding to the higher abundance of *Sulfurimonas* transcripts observed at these vents (Fig 3). Two bins classified as *Hydrogenimonas* (bins 102 and 104) were transcribed across different temperatures and vents. Bin 102 was transcribed only at Marker 33 at 30°C, but at 55°C, bin 102 was transcribed at all vents in at least one timepoint. Bin 104 transcripts, however, were observed only at 30°C at Anemone. Nautiliaceae bin 340 transcripts were ubiquitous at 55°C at nearly all sites and years. *Methanothermococcus* bin 335 transcripts were found at 55°C at only Marker 113 and Marker 33 in 2013, while no methanogen populations were transcribed at Anemone (Figs 3 and 4).

In general, MAGs expressed a higher proportion of their coding genomes in the 80°C experiments, compared to the other temperatures. *Thermovibrio* bins (bin 320 and bin 374) were transcribed across all 80°C experiments, matching the high abundance of the genus in the transcripts at all vents (Figs 3 and 4). The Desulfurobacteriaceae bin 324 was transcribed in 2014 at all sites at 80°C. Aquificales bin 285, however, was restricted to only Anemone (Fig 4).

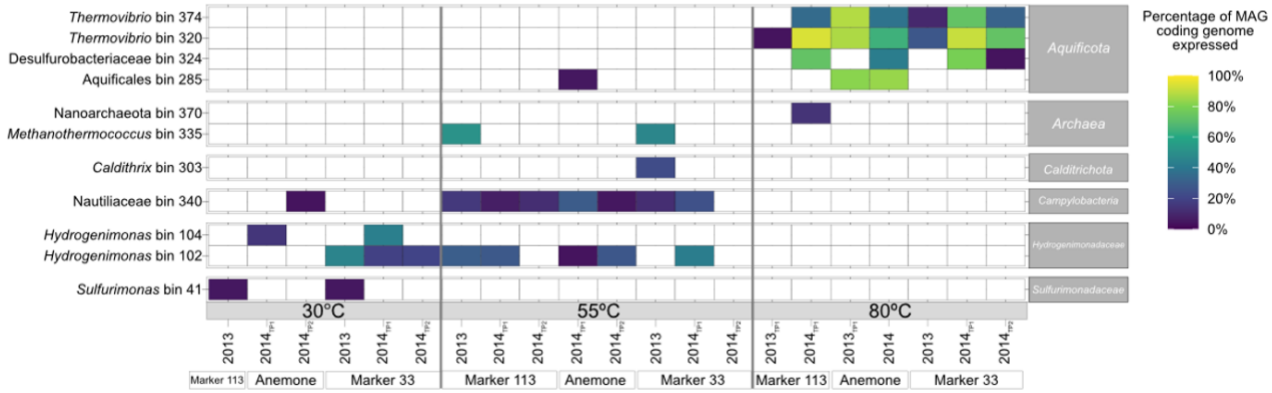

Figure 4. Metagenome Assembled Genomes (MAGs) selected based on having >4% of coding genome expressed in 30, 55 and 80°C ^{13}C-enriched fraction of RNA-SIP experiments. Percent of coding genome expressed = length of expressed genes(bp)/genome length (bp).

Functional attributes of ^{13}C-enriched active autotrophs

To determine how autotrophs in the ^{13}C-enriched fraction of RNA-SIP experiments acquired energy while taking up labeled bicarbonate, we identified transcripts for key genes involved in oxygen, nitrogen, methane, hydrogen, sulfur, and carbon fixation pathways, and compared those to the unmanipulated fluid metatranscriptomes (Fig 5, Table S7). There were similarities in major energy acquisition pathways across all sites and samples, but in each year and temperature, the three vent sites differed in magnitude of transcription. Transcripts for the selected metabolic marker genes were present in most of the unmanipulated fluid metatranscriptomes (Fig

310 5), whereas some genes were transcribed in the ^{13}C-enriched fraction of the RNA-SIP
311 metatranscriptomes only at certain temperatures and vents, reflecting specific metabolisms being
312 carried out by distinct subseafloor autotrophic populations under different temperature regimes.
313 We also examined the 30 most abundant transcripts at each RNA-SIP experimental temperature
314 (Fig S8), some of which were metabolic genes that we note here, while other transcripts were
315 related to information processing, replication and repair, and signaling and cellular processes (Fig
316 S8).

317 Transcripts for aerobic oxidative phosphorylation gene *aa3*-type cytochrome c oxidase
318 (*cox*) and microaerophily gene *cbb3*-type cytochrome c oxidases (*cco*) were highest in the ^{13}C-
319 enriched fraction of the 30°C RNA-SIP experiments as compared to 55 and 80°C (Fig 5).
320 Normalized counts of *cco* peaked at Marker 33 at 30°C in both 2013 and 2014 (7,593–9,608 TPM),
321 attributable to taxa *Aliarcobacter*, *Hydrogenimonas*, *Sulfuricurvum*, *Sulfurimonas*, and
322 *Sulfurovum* (Table S8).

323 Genes for nitrate reduction and complete denitrification were highly transcribed in almost
324 all the ^{13}C-enriched fraction of the RNA-SIP metatranscriptomes (Fig 5). Of those genes, *napA*,
325 periplasmic nitrate reductase, was the most abundant transcript across all conditions. It was also
326 one of the 30 most transcribed genes at 80°C (1,394–15,195 TPM) (Figs 5 and S8), belonging to
327 the genera *Phorcysia* and *Thermovibrio* within the Aquificota. Marker 113, and to a lesser extent,
328 Marker 33, had transcription of genes for dissimilatory nitrate reduction to ammonia (DNRA;
329 *nirAB* and *nrf*, TPMs 8,131–16,106), and these transcripts were uniquely attributed to
330 *Sulfurospirillum* (Table S8).

331 Of the six sulfur marker genes selected, *psr* and *phs* are most functional in anaerobic
332 conditions and *sox* in aerobic conditions (31). However, many sulfur metabolism genes can

333 function across diverse oxic conditions, as they catalyze both anaerobic sulfate reduction and the
334 reverse process, sulfur-compound oxidation (32, 33). Anemone had the highest H_2S concentrations
335 (Table 1) as well as transcription of genes related to sulfur metabolism compared to the other two
336 vents (Fig 5). For example, *sqr* had high transcription at 80°C (up to 9,695 TPM from *Aquifex*,
337 *Hydrogenivirga*, and *Phorcysia*), whereas at both Marker 113 and Marker 33, *sqr* was transcribed
338 only at 30°C and 55°C (Fig 5). The highest transcription of polysulfide/thiosulfate reductase genes
339 *psr* and *phs* occurred at 55°C in all experiments, with transcripts reaching 27,947 TPM from
340 *Hydrogenimonas*, *Cetia*, and *Nautilia* (Fig S8). While *sox* transcripts were present in
341 unmanipulated fluids at all three vents, activity of this gene in the ^{13}C-enriched RNA-SIP
342 metatranscriptomes was highest in 2014 at Marker 33 at 30°C (6396 TPM) from *Hydrogenimonas*,
343 *Sulfurovum*, and *Sufurimonas* (Table S8).

344 The selected marker genes for methanogenesis were transcribed in the unmanipulated fluid
345 samples from Marker 113 and Marker 33 but were overall absent at Anemone (Fig 5).
346 Transcription of methanogenic metabolic genes was highest in the ^{13}C-enriched RNA-SIP
347 metatranscriptomes from Marker 113 in 2013 at 55°C and 80°C (up to 56,765 TPM), and Marker
348 33 at 55°C in 2013 and at 80°C in 2014 (up to 47,489 TPM). These transcripts were attributed to
349 *Methanothermococcus* and *Methanococcus* at 55°C and *Methanotorris* and *Methanocaldococcus*
350 at 80°C. Methanogenic genes *hdrA2* and *mcrA* at 55°C and *frhA*, *fwdB*, *fmdB*, and *mcrAC* at 80°C
351 were among the 30 most transcribed genes in these temperatures (Fig S8).

352 The five chosen hydrogenase marker genes were in all unmanipulated fluid
353 metatranscriptomes (Fig 5). Notably, throughout all sites and all years, the ^{13}C-enriched
354 transcriptional profiles from 80°C RNA-SIP experiments did not have quinone-reactive Ni-Fe
355 hydrogenase *hydAB,* responsible for transferring electrons from H_2 to terminal electron acceptors

356 oxygen, nitrate, sulfate, fumarate, and metals (32). Transcripts for *hydAB* in the 30°C and 55°C
357 experiments belonged to diverse Campylobacterota, predominantly *Sulfuricurvum* (22,883 TPM,
358 Table S8), but also *Sulfurimonas*, *Nautilia*, and *Hydrogenimonas.* Other hydrogen metabolic
359 marker genes, such as sulfhydrogenase, energy converting (*ech*) hydrogenase and Ni-Fe
360 hydrogenase (group 1; *hya*, *hyb*), were in higher abundances at 55°C and 80°C compared to 30°C
361 and associated with *Thermococcus* and Phylum Aquificota (Table S8). F420-non-reducing
362 hydrogenase (*mvh*, *vhu*, *vhc*) used by methanogens was primarily at Marker 113 and 33 at 55°C
363 and 80°C. Some of these hydrogenase marker genes were among the top 30 genes transcribed in
364 the respective temperatures in the dataset (Fig S8).

365 Across all ^{13}C-enriched RNA-SIP metatranscriptomes at 30°C and 55°C, most of the
366 carbon fixation was via the reductive tricarboxylic acid (rTCA) cycle (Fig 5), with high
367 transcription of rTCA cycle marker genes attributed to Campylobacterota (Table S8). At 80°C in
368 both years at Anemone and in 2014 at Marker 113 and Marker 33, rTCA transcripts were attributed
369 to Aquificota (Fig 5, Table S8). Eight genes involved in the rTCA/TCA cycles were among the 30
370 most abundant genes transcribed at each temperature (Fig S8). At Marker 113 (2013) and Marker
371 33 (2014; Tables S7 and S8), in experiments at 80°C when methanogens were active, transcripts
372 for the reductive acetyl-coA (Wood-Ljungdahl) pathway were also abundant, including Wood-
373 Ljungdahl pathway genes (*coo, acs*) attributed to *Methanocaldococcus*.

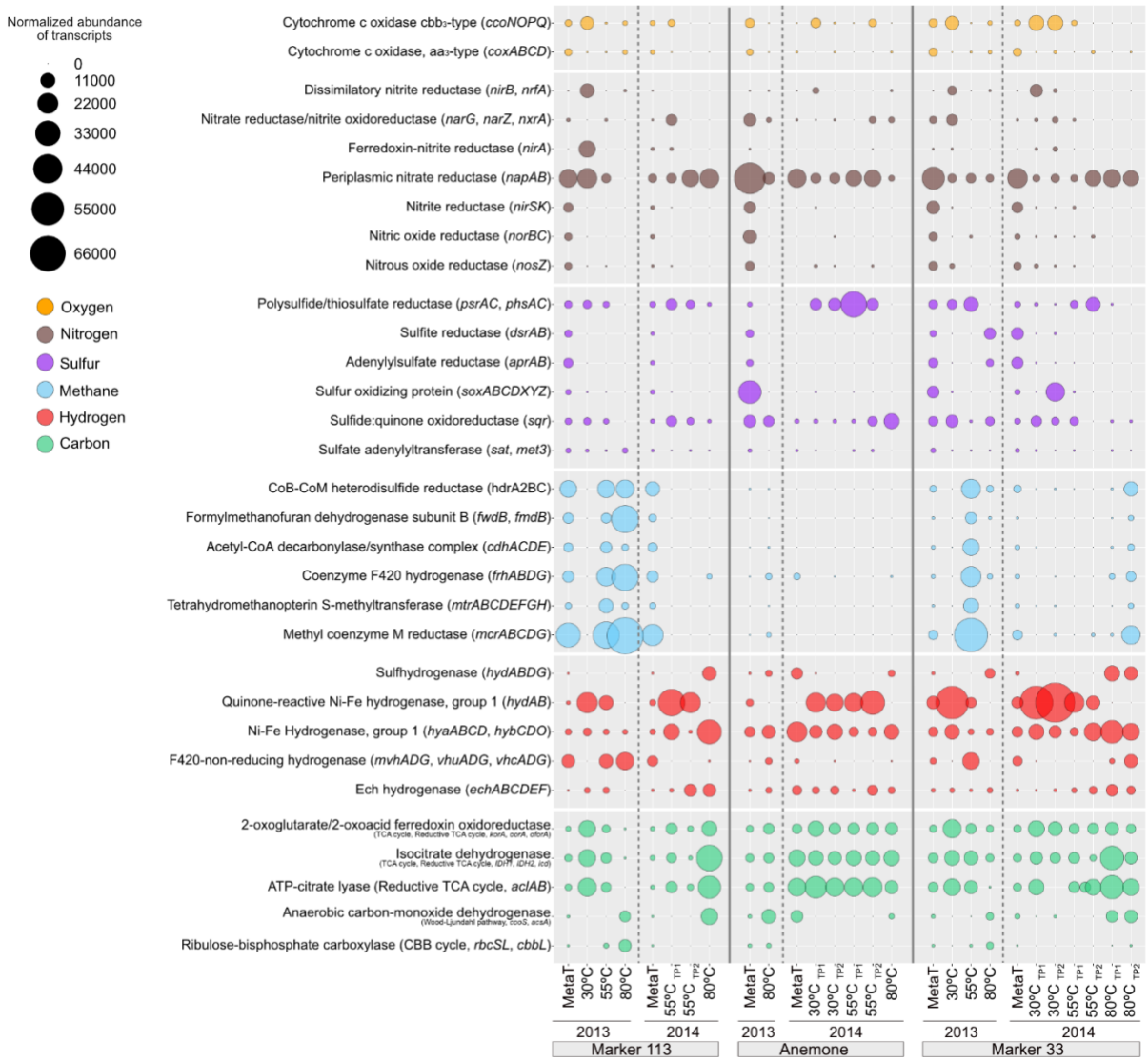

Figure 5. Normalized abundance of non-rRNA transcripts annotated in the unmanipulated diffuse fluid metatranscriptomes ("MetaT") and ^{13}C-enriched fractions of RNA-SIP metatranscriptomes for key marker genes involving oxygen, nitrogen, sulfur, methane, hydrogen, and carbon fixation. Bubble sizes represent the transcripts per million reads (TPM) attributed to each marker gene.

Differential Expression Analysis of ^{13}C-enriched Transcripts

Differential expression analyses using the RNA-SIP ^{13}C-enriched transcriptional profiles were conducted to determine statistical differences in transcription across experimental conditions

383 without bias towards any specific functional annotations. Due to the absence of an untreated
384 control in our dataset, an iteration of differential expression analysis was used that does not require
385 an untreated control; instead, expression profiles were compared to a baseline "expected"
386 transcription calibrated to each comparison of interest (34-38). In this study, comparisons were
387 made across temperatures within each vent, across temperatures among the three different vents,
388 and between years within each vent (see Methods and Supplementary Methods; 34-38). Across all
389 ^{13}C-enriched RNA-SIP metatranscriptomes, 656 unique transcripts were observed to be
390 significantly differentially expressed (SDE) 1520 times with an adjusted p-value of <0.05 (Table
391 S9). Only genes that had a padj < 10^{-3} and $\log_2$ fold-change ≥ |2| will be discussed.

392 When comparing across temperatures within each vent, the highest number of transcripts
393 were significantly differentially expressed (483 unique genes SDE 1030 times, Fig 6, Table S10).
394 The baseline for this comparison was the average expression of all ^{13}C-enriched RNA-SIP
395 metatranscriptomes (n=21; Table 2). Within Marker 113, annotated transcripts with the greatest
396 differences in expression across temperatures included gene transcripts for hydrogen metabolism,
397 nitrate reduction, and carbon fixation (Fig 6A). At Marker 113, as RNA-SIP experimental
398 temperature increased, the differentially expressed hydrogenase transcripts in the ^{13}C-enriched
399 fraction shifted from quinone-reactive Ni-Fe hydrogenases (*hyd*) being overexpressed at 30°C and
400 55°C and underexpressed at 80°C, to Ni-Fe hydrogenase (group 1) (*hya*, *hyb*) being overexpressed
401 at 80°C and underexpressed at 30°C. The hydrogenases *mvh*, *vhu,* and *vhc*, utilized in
402 methanogenesis, were also underexpressed at 30°C.

403 At Anemone, transcribed genes with the greatest differences in abundance across
404 temperatures included transcripts related to carbon fixation and hydrogen, methane, nitrogen, and
405 sulfur metabolism (Fig 6B). At 55°C, Calvin-Benson-Bassham (CBB) cycle genes *rbc* and *cbb*

were underexpressed. The hydrogen metabolism genes *hyd*, *hya*, and *hyb* followed the same pattern of differential expression as at Marker 113. At all temperatures at Anemone, transcripts for genes involved in oxygen-sensitive methanogenesis (*mvh*, *vhu, vhc; frh*, *fdh*, and *hdr*) were underexpressed. Nitrate reduction gene *nap* was underexpressed at 80°C, while the nitrite reduction gene *nrf* was overexpressed at 55°C. Finally, sulfur metabolism genes for polysulfide/thiosulfate reduction (*phs*, *psr*) were underexpressed at 80°C and overexpressed at 55°C (Fig 6B).

There were more differentially expressed transcripts across temperature within Marker 33 than the other vents, reflecting the greater number of metatranscriptomes in the dataset (n=9 ^{13}C-enriched RNA-SIP metatranscriptomes, Table 2). These included transcripts for hydrogen, methane, nitrogen, and sulfur metabolism (Fig 6C). Marker 33 had the same pattern for differential expression of hydrogenases *hyd*, *hya*, and *hyb* as both Marker 113 and Anemone. A gene for methanogenesis, *frh*, was underexpressed at 55°C. Marker 33 had the same genes differentially expressed in the same pattern as Anemone for nitrogen and sulfur metabolism.

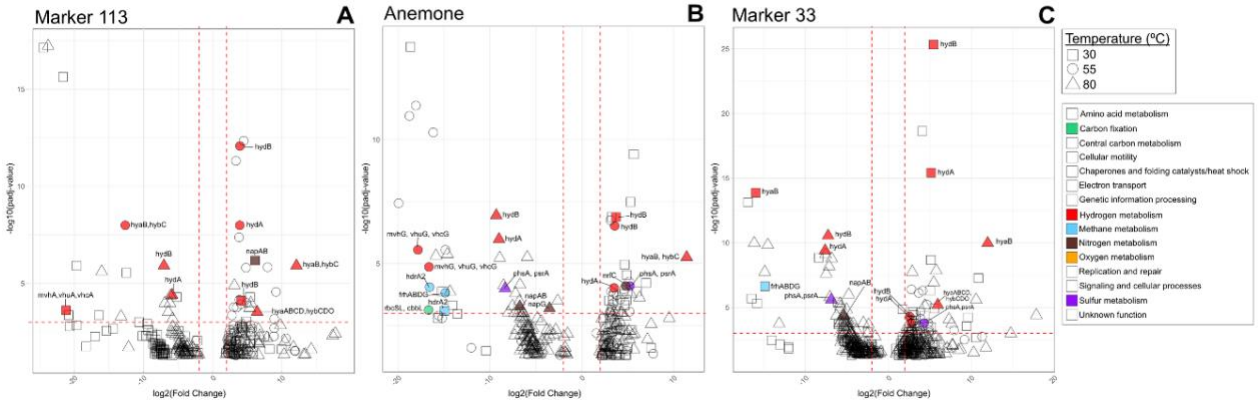

Figure 6. Volcano plots showing the $\log_2$FC (degree of differential expression) across experimental temperatures at each vent **A.** Marker 113, **B.** Anemone, and **C.** Marker 33. Colored and labeled points correspond to genes involved in carbon fixation, hydrogen, methane, nitrogen, oxygen, and sulfur metabolism that had a padj < 10^{-3} and $\log_2$FC > |2| [padj; p-value adjusted for multiple tests using the Benjamini-Hochberg procedure to control the false discovery rate (FDR)].

When comparing across vents by temperature (Fig S10), 240 transcripts were significantly differentially expressed 329 times, using a baseline expression of normalized transcript counts of all ^{13}C-enriched RNA-SIP metatranscriptomes within each temperature (n=6 for 30°C, n=8 for 55°C, and n=9 for 80°C; Table 2). This comparison revealed SDE transcripts for genes related to hydrogen and nitrogen metabolism. At 30°C, nitrate and nitrite reduction genes *nap* and *nir* were overexpressed only at Marker 113, while nitrate/nitrite reduction genes *nar*, *nxr* were overexpressed at Marker 33 (Fig S10, Table S11). The greatest number of significantly differentially expressed transcripts was observed at 30°C. None were identified at 55°C, and only three transcripts were significantly differentially expressed in the 80°C experiments.

In a comparison between 2013 and 2014 within each vent, 114 unique genes were significantly differentially expressed 161 times (Fig S11, Table S12). The baseline expression for

442 this analysis was the same that was used for the across vents by temperature comparison, but the
443 contrast in DESeq2 was switched to time instead of temperature (see Methods). Most SDE genes
444 were overexpressed at Marker 113 and Marker 33 in 2013, including a Wood-Ljungahl pathway
445 carbon fixation gene (*cdh*) and methanogenesis hydrogenase genes *mvh*, *vhu*, and *vhc* at Marker
446 33 and several other methanogenesis genes at both Marker 113 and 33. For Figures with additional
447 significantly differentially expressed genes coded and annotated by general functional categories,
448 see Figures S9, S10 (D-F), and S11 (D-F).

449 **DISCUSSION**

450 In this study, we experimentally manipulated venting fluids to target subseafloor microbes
451 under variable temperature conditions and used stable isotope labeling with inorganic carbon
452 coupled to metatranscriptomic sequencing to focus on active autotrophic subseafloor microbes,
453 their metabolic and growth strategies, and their distribution in the subseafloor. Expanding upon
454 decades of research at Axial Seamount, we analyzed 15 RNA-SIP experiments from three spatially
455 separated vents in two consecutive years and hypothesized that the subseafloor autotrophic
456 microbial population structure at each site and temperature would be distinct, with transcriptional
457 metabolic profiles reflective of the geological and geochemical characteristics of each individual
458 vent. While our results broadly corroborate this hypothesis and build upon previous work at Axial
459 Seamount that indicated microbial communities at individual vents host distinct microbial
460 communities over multiple years (10, 12), by focusing on only autotrophs at specific temperatures,
461 we also found active, cosmopolitan (found at all sites, regardless of vent geology), subseafloor
462 autotrophs occupying particular thermal niches. In addition, while certain metabolisms and
463 associated lineages such as methanogenic archaea ("specialists") are restricted in distribution,
464 other metabolisms geared toward hydrogenotrophic sulfur and nitrate utilization and

465 microaerophily ("generalists") are widely distributed in many lineages across a wide temperature
466 range, highlighting metabolic flexibility and functional redundancy across diverse taxonomic
467 groups in this ecosystem. Competition for electron donors like hydrogen and electron acceptors
468 like oxygen was apparent in the data, as shifts in taxonomy and transcription highlighted the
469 conditions under which various microbial groups could dominate. The data suggest that while
470 chemical and physical characteristics at each vent control the energy available for microbial
471 growth—as is the case for methanogenesis and sulfide oxidation—some ubiquitous microbial
472 subseafloor lineages within the young oceanic crust at Axial Seamount have adapted to a broad
473 range of subseafloor chemistries and temperatures and are therefore not restricted in distribution.

474 All ^{13}C-enriched fractions of the RNA-SIP experiments experienced a significant
475 distillation of the taxa present in the unmanipulated fluid metatranscriptomes (Fig 3). Of note is
476 the reduction or disappearance of *Alpha*-, *Delta*-, and *Gammaproteobacteria*, as well as
477 *Actinobacteria*, groups that comprised up to half of the microbial community in unmanipulated
478 fluids and are common in plume and background seawater samples. The RNA-SIP experiments
479 were amended with hydrogen to re-create likely energy-rich, warm subseafloor conditions, based
480 on both cultivation experiments from Axial (39) as well as failed RNA-SIP experiments without
481 hydrogen enrichment (8). Along with temperature of incubation, this likely explains why these
482 common deep ocean taxa are not heavily represented in the ^{13}C-enriched RNA-SIP
483 metatranscriptomes, as they are either not adapted to these subseafloor conditions or are
484 heterotrophs. Here, we discuss some of the specific patterns of taxonomic distribution coupled
485 with the gene expression patterns and geochemical features across the three vents to determine
486 how the interplay of fluid chemistry, microbial competition, and functional potential results in the
487 presence or absence of microbial populations across vents and temperatures.

488 The novel *in situ* oxygen sensor data enabled new insights into the important role of oxygen
489 for subseafloor microbial metabolism, even at high temperatures. Through linear regression
490 modeling of this data, we predicted oxygen was depleted to zero at temperatures of 33°C at Marker
491 113 and 52°C at Marker 33 but was predicted to be present at temperatures up to 100°C or more
492 at Anemone (Fig 1). These oxygen models align with the transcript data, as the presence of oxygen
493 at high temperatures at Anemone likely enabled the persistence of microaerophilic sulfide
494 oxidation in 80°C experiments. This was indicated by the transcription of sulfide:quinone
495 oxidoreductase (*sqr*) for sulfide oxidation belonging to *Aquifex*, *Hydrogenivirga*, and *Phorcysia*.
496 However, at Marker 113 and Marker 33, this oxygen-dependent enzyme for autotrophy (40) was
497 not expressed above 55°C, consistent with the depletion of oxygen at lower temperatures at these
498 sites.

499 At all sites in all years, the geochemistry of the diffuse venting fluids indicated biological
500 utilization of hydrogen when compared with conservative mixing, with evidence for methane
501 production only at Marker 113 and Marker 33 (Fig 2). These geochemical indicators of biological
502 activity broadly map to the metabolism-focused analyses. ^{13}C-enriched transcripts for
503 methanogenesis, an anaerobic metabolism, were restricted to Marker 113 and 33 (Fig 5). In
504 addition, the top 30 expressed genes (TPM) at 55°C and 80°C included those related to
505 methanogenesis only at these two vents (Fig S8). This also corresponds to the consistent activity
506 of the singular, high quality *Methanothermococcus* MAG (bin 335) at Marker 113 and 33 (Fig 4).
507 In contrast, at Anemone, methanogenesis-related ^{13}C-enriched transcripts were not included in the
508 top 30 expressed genes (Fig 5 and S8), and were overall significantly underexpressed compared to
509 other sites, likely due to the more oxic conditions measured at this site (Figs 1 and 5).

510 Unlike the restricted distribution of transcripts for methanogenesis, all sites showed

511 biological utilization of hydrogen, and at Marker 113 and 33, also utilization of nitrate (Fig 2).
512 ^{13}C-enriched transcripts for hydrogen and nitrate utilization were found widely across all
513 conditions, and in particular, the periplasmic nitrate reductase *napAB* and hydrogenase genes
514 quinone-reactive Ni-Fe hydrogenase (*hyd*), energy-converting hydrogenase (*ech*), and Ni-Fe
515 hydrogenase (group 1) (*hya*, *hyb;* Fig 5) were all overexpressed in the differential expression
516 analysis. The transcripts for hydrogen oxidation coupled with nitrate reduction were associated
517 with a diverse number of genera, including *Sulfurimonas, Cetia, Hydrogenimonas,* and
518 *Caminibacter* at 30°C; *Cetia, Caminibacter, Nautilia, Hydrogenimonas* and those from phylum
519 Aquificota at 55°C; and *Thermovibrio* and *Desulfurobacterium* at 80°C (Fig 3). Chemical analysis
520 of diffuse fluids showed that there was higher H_2S concentrations in both 2013 and 2014 at
521 Anemone than at the other two vents (Tables 1 and S1), correlating with high transcription of
522 polysulfide/thiosulfate reduction genes *psr* and *phs* (up to 14,000 TPM) in tandem with hydrogen
523 oxidation (Fig 5). Taxa expressing both *psr* and *phs,* along with quinone-reactive Ni-Fe
524 hydrogenase at Anemone, include *Cetia, Nautilia*, and *Hydrogenimonas*; the latter is known to
525 utilize oxygen as a terminal electron acceptor (41).

526 Within each year, there were also MAGs active in all vents in at least one time point:
527 *Hydrogenimonas* bin 102 (at 55°C in 2014), Nautiliaceae bin 340 (at 55°C in 2013 and 2014),
528 *Thermovibrio* bin 320 (at 80°C 2013 and 2014), and Desulfurobacteriaceae bin 324 (at 80°C in
529 2014). The recurrence of active MAGs across vents and temperatures indicated that some vents at
530 Axial Seamount host the same populations of microorganisms, agnostic of vent geology (basalt
531 vs. sulfides) or geochemistry (Fig 4). Previous studies (e.g. 9-10, 16, 42) determined that
532 established subseafloor microbial communities are mostly restricted by local vent fluid
533 geochemistry and physical structuring of the site. For example, Fortunato *et al*., (2018) showed

534 MAGs identified as mesophilic and thermophilic methanogens were restricted mainly to Marker
535 113 and not Marker 33 or Anemone. This result is connected to both vent chemistry (hydrogen,
536 methane concentrations) and physical mixing, allowing for a more stable subseafloor community
537 compared to other vents (10). However, our results show this may not be true for all lineages at
538 the population level. Our data reveal that some cosmopolitan taxa are capable of colonizing a wide
539 range of environmental niches, functioning as ecosystem generalists. On the other hand, lineages
540 restricted in distribution, such as methanogens, serve as an example of ecosystem specialists.

541 Many of these cosmopolitan taxa that carry out hydrogenotrophic sulfur and nitrate
542 reduction are known to be efficient at oxidizing hydrogen. For example, a study done by Nishimura
543 *et al*. (2010) found that hydrogenases purified from the vent-endemic *Hydrogenimonas*
544 *thermophila* were phylogenetically related to pathogenic Campylobacterota, known to have high
545 hydrogen oxidation activity (43). Like *Hydrogenimonas,* another vent-endemic organism *Nautilia*
546 *profundicola* was found to have multiple operons for hydrogenases, including one H_2-sensing
547 (Group 2), two H_2-uptake (Group 1), and three H_2-evolving (Group 4) hydrogenases in their
548 genome. Consistent with the findings from cultured representatives of *Hydrogenimonas* and
549 *Nautilia* that highlight flexibility encoded in their genomes for hydrogen utilization (44), our MAG
550 analyses indicated that bins taxonomically identified as *Hydrogenimonas* and *Nautilia* transcribed
551 three of the four hydrogen marker genes at 55°C, including quinone-reactive Ni-Fe hydrogenase
552 (*hyd*), Ni-Fe hydrogenase (group 1) (*hya, hyb)*, and energy converting hydrogenase (*ech*; Table
553 S13).

554 Transcripts for hydrogenases were also detected at 80°C at both the community level and
555 in the ubiquitous Aquificota MAGs, supporting the prevalence and importance of hydrogen
556 oxidation in these taxa. Transcripts for three hydrogenase marker genes, Ni-Fe hydrogenase (group

557 1) (*hya*, *hyb*), energy-converting hydrogenase (*ech*), and sulfhydrogenase, are attributed to both
558 *Desulfurobacterium* and *Thermovibrio* (Figs 3 and 5, Table S8). Desulfurobacteriaceae bin 324
559 was present at all vents in 2014 and was found to transcribe the hydrogenase maturation gene *hypF*
560 (Table S13). *Thermovibrio* bin 374, found at all vents in 2013 and 2014, transcribed numerous
561 hydrogenases, including an F420-non-reducing hydrogenase, hydrogenase maturation gene *hypF,*
562 hydrogenase expression/formation genes *hypED*, and multiple sulfhydrogenase subunits (Table
563 S13). The diversity and versatility of these hydrogenase genes likely enable these taxa to grow and
564 survive across vents with different chemistries, leading to the cosmopolitan nature of these
565 populations.

566 Hydrogen is also utilized by hydrogenotrophic methanogens at these vents, and
567 competition for hydrogen among methanogens and the cosmopolitan, hydrogenotrophic sulfur and
568 nitrate reducers of the Aquificota likely occurs in the subseafloor at temperatures >50°C (45-47).
569 Methanogenic growth may be inhibited by growth of these other groups by bringing localized H_2
570 concentrations to a partial pressure below which methanogenesis can occur (48-50). Cultivation
571 experiments showed that *Desulfurobacterium* strain HR11 has a lower H_2 requirement and lower
572 K_s than *Methanocaldococcus* (30 μM vs. 67 μM; 39, 46, 47). In co-culture experiments with
573 *Methanothermococcus thermolithotrophicus* (T_{opt} 65°C), *Methanocaldococcus jannaschii* (T_{opt}
574 82°C), and *Desulfurobacterium thermolithotrophum* (T_{opt} 72°C), Kubik and Holden (2024) found
575 that *D. thermolithotrophum* outcompeted both methanogens at high and low hydrogen
576 concentrations when grown at a 1:1 ratio of initial inoculum (45). However, when *M.*
577 *thermolithotrophicus* was grown at a ratio of 10:1 with *D. thermolithotrophum*, the methanogen
578 outcompeted the bacterium, suggesting the conditions under which methanogens can successfully

579 establish first and grow in larger numbers, as observed in the 55°C experiments at Markers 113
580 and 33 where methanogens were in higher abundance.

581 An additional factor that can influence the distribution and metabolic strategies of
582 hydrogen-utilizing microbes are physical characteristics of the hydrothermal vents. Building off a
583 reactive transport model developed to examine thermophilic versus hyperthermophilic
584 methanogen growth at Axial vents (28), Kubik and Holden expanded the model with additional
585 hydrogenotrophic autotrophs and determined that when the residence time of subseafloor fluids
586 was long, methanogens dominated, but when fluids had shorter residence times, Aquificota
587 dominated. Lower temperatures combined with longer residence times also favored thermophilic
588 methanogenic growth (45). Taken together, our results support these cultivation and modeling
589 studies and show that in the natural world, methanogens require more specific physicochemical
590 conditions for successful growth, thus limiting their distribution, whereas diverse Aquificota and
591 Campylobacterota are more metabolically flexible and less dependent on geochemistry
592 constrained by fluid residence times, enabling a more cosmopolitan distribution. Anemone's close
593 (<1 m) proximity to a high temperature (~300°C) end-member may create short subseafloor fluid
594 residence times; in contrast, Marker 113 and Marker 33 are located farther (~750 m) from a high-
595 temperature venting source, supporting longer fluid residence times, and thus methanogens (28).
596 Our coupled geochemical and meta-omics results suggest that the distribution of some subseafloor
597 microbes may be determined by both a microbe's efficiency and genetic regulation of hydrogen
598 utilization as well as the interspecies relationships, chemistry, residence time, and temperature of
599 the subseafloor venting fluids.

600 Microbial community composition shifted with temperature and vent location.
601 Campylobacterota dominated all ^{13}C-enriched RNA-SIP metatranscriptomes until 80°C, when

602 methanogens and members of the Aquificota became the key carbon-fixing phyla. At 30°C, ORF-
603 based transcript analysis attributed a substantial proportion of transcripts to *Sulfurimonas* at
604 Marker 113 and *Hydrogenimonas* at Marker 33 (Fig S12). Fluid chemistry may explain why these
605 genera are the dominant autotrophs in these low-temperature conditions at each respective vent.
606 Diffuse fluids in both Marker 113 and Marker 33 had comparable H_2 concentrations across the
607 years, though 10x lower than those in Anemone, but the oxygen-temperature trends observed in
608 water samples predicted zero-oxygen (anoxia) at temperatures above 55°C (Fig 1). In our study,
609 *Sulfurimonas* was especially active and abundant in Marker 113 at 30°C. The O_2 concentration
610 measured at Marker 113 was consistently the lowest of all three vents each year (7.0 µM in 2013,
611 9.9 µM in 2014, Fig 1, Table 1). While fluid residence times and flow rate impact oxygenation,
612 Marker 113's comparatively low oxygen concentrations may be in part due to *Sulfurimonas* O_2
613 consumption. In the 30°C expression profiles of Marker 113 and Anemone, *Sulfurimonas* only
614 transcribed the cytochrome c oxidase gene, *cbb*$_3$-type (*ccoNOPQ*) and no other genes for
615 alternative electron acceptors suggestive of a metabolism of oxygen reduction and hydrogen
616 oxidation (Figs 5 and S12, Table S8). Given the absence of *Hydrogenimonas* metabolic transcripts
617 and the overall dominance of *Sulfurimonas* in transcriptional profiles of Marker 113 at 30°C, the
618 depleted activity of microaerophilic *Hydrogenimonas* may reflect more stringent conditions (e.g.
619 less H_2 and less O_2), and/or competition with *Sulfurimonas* for oxygen as an electron acceptor. On
620 the other hand, the metabolic versatility and higher growth optimum temperature of
621 *Hydrogenimonas* may provide for its continued activity level at higher temperatures, where it can
622 utilize alternative electron acceptors such as nitrate, nitrite, and sulfur (51). In our experiments,
623 *Hydrogenimonas* were more abundant at all sites at 55°C compared to 30°C.

However, at Marker 33, *Sulfurimonas* and *Hydrogenimonas* were present in nearly equal proportion in the 30°C transcriptional profiles for both years. Both taxa utilize the same electron acceptors, except for sulfur compounds and thrive in microaerophilic conditions (Fig S12, Table S13; 51-53) The presence of oxygen up to 52°C at Marker 33, closer to the growth optimum of *Hydrogenimonas,* suggests that both *Sulfurimonas* and *Hydrogenimonas* can use oxygen at higher temperatures at this site (Fig 1, Table S2). On the other hand, these sustained oxygen concentrations up to 52°C may also hinder establishment of taxa with similar metabolisms, higher optimum growth temperature, but lower oxygen tolerance than *Hydrogenimonas* (e.g. *Caminibacter, Cetia, Lebetimonas*, and *Nautilia*).

Conclusions

This study identified subseafloor microbial primary producers at three spatially separated diffuse vents over two years at Axial Seamount and enabled a granular view of the autotrophic microbes at the base of the deep-sea hydrothermal vent ecosystem. The active autotrophs vary among vents, demonstrating that vent geology, fluid chemistry, and flow path shape the geochemical environments and active metabolisms observed. This dynamic interplay between microbial metabolism and vent fluid chemistry not only influences the community structure but also determines which groups dominate under varying environmental conditions. Hydrogen and oxygen availability and utilization is a key control for the establishment of autotrophs, with competition between autotrophic sulfur-reducing taxa and methanogens for hydrogen evident. These interactions underscore the complex ecological networks at hydrothermal vents, where microbial communities not only adapt to but also actively shape their environment through metabolic exchanges and niche differentiation.

647 **MATERIALS AND METHODS**

648 *Sample collection*

649 Axial Seamount (Fig S1) samples were collected using ROVs ROPOS and JASON aboard the
650 *R/V Falkor* and *R/V Thompson* in September 2013 and *R/V Brown* in August 2014 (8, 10).
651 Hydrothermal plume water from 42 m above Anemone (N 45.9335667, W 130.013667) and
652 ambient seawater at 1500 m depth (N 46.27389, W 129.79548) were also collected using a Seabird
653 SBE911 CTD equipped with 10 L Niskin bottles in 2015 aboard the *R/V Thompson*, 5-months
654 post-eruption at Axial Seamount. Water was transferred from Niskin bottles into expandable
655 plastic containers, and 3 L was filtered through 0.22 µm Sterivex filters (Millipore, Billerica, MA,
656 USA) for metagenomic sequencing only.

657 The Hydrothermal Fluid and Particle Sampler (HFPS; 27) and Large Volume Water
658 Sampler (LVWS; 54) were used to collect fluids at ~2 cm above the seafloor. The coordinates for
659 each vent are Marker 113: N 45.9227, W 129.9882; Anemone: N 45.9332, W 130.0137; Marker
660 33: N 45.9332, W 129.9822. Temperature was monitored while drawing fluids using an integrated
661 temperature sensor that was present on both samplers. For sampling with the HFPS and LVWS, a
662 4 L capacity acid-washed Tedlar bag or a 5 L acid-washed plastic carboy, respectively, was used
663 to collect fluids for RNA-SIP experiments as described in (8). DNA and RNA from diffuse fluids
664 for metagenomic (2013-2015) and metatranscriptomic (2013 and 2014) sequencing were
665 concurrently collected using the HFPS at a rate of 100–150 mL min^{-1} through a 0.22 µm, 47 mm
666 GWSP filter (Millipore) on the seafloor for a total volume of 3 L. All filters were preserved *in situ*
667 with RNALater (Ambion, Grand Island, NY, USA) as described in Fortunato *et al*. (2018) (10).
668 RNA-SIP experiments are reported here only from 2013 and 2014, since there were too few
669 samples from 2015 to include in the analysis, though the unmanipulated diffuse fluid metagenomes

670 were included in the assemblies to provide more phylogenetic and functional coverage
671 representative of the Axial diffuse fluid microbial community.

672 Hydrothermal fluid samples were collected with the Hydrothermal Fluid and Particle
673 Sampler (HFPS) following procedures described in (27). Vent fluid samples were analyzed on
674 board for pH, total H_2S, and dissolved methane and hydrogen. Magnesium and nitrate were
675 analyzed on shore. With the exception of oxygen data, these chemical data were previously
676 reported in (10) and used for methanogen modeling in (28). For this study, HFPS included an
677 oxygen optode (SeaBird SBE 63) capable of measuring oxygen concentration in fluids up to a
678 maximum of 40°C. Temperature was monitored at the sample intake, near the sensor block, and
679 inside the oxygen sensor housing. Oxygen measurements were made just before or after collecting
680 fluid samples, with the intake in the same position to replicate collected water samples. Water was
681 pulled from the titanium/Teflon sampling manifold through the sensor, with some cooling taking
682 place along the flow path. The SBE63 optode does not require a constant flow rate, does not
683 consume oxygen, and can make measurements when flow is stopped. The SBE63 sends 1 Hz serial
684 data, which is received by the HFPS on-board computer. Oxygen concentration is calculated using
685 the temperature measured in the sensor housing, the ambient pressure and salinity (derived from
686 ROV sensors and input manually to the software), and the factory calibration, which covers a
687 temperature range from 2°C to 30°C. All the measurements for this study had temperatures at the
688 sensor within the calibration range. Over the 2013-2015 period of this study, the average oxygen
689 concentration of near-bottom seawater within the caldera, where all diffuse vents for this study are
690 located, was 31 µmol/kg (+/- 2µmol/kg, n=24, Fig 1, Table S2). Oxygen increases significantly
691 with increasing depth at Axial Seamount, where the summit is below the oxygen minimum.

692 *RNA-SIP experimental procedures*

Carboys and Tedlar bags were recovered from the ROV and brought to the shipboard lab, where filling into evacuated bottles began immediately. Both were kept at ambient temperature during filling and remained sealed to minimize oxygen exposure, although some likely occurred. The Tedlar bag was housed in a water filled plastic cylinder for collection. As the bag was emptied during bottle filling, additional water was pumped into the cylinder to keep pressure on the bag and minimize outgassing. The time between ROV recovery and experimental set-up was less than 1 hour. For LVWS samples in 2013, fluid from carboys was pumped using a peristaltic pump into evacuated 1 L Pyrex bottles with air-tight butyl stoppers to a volume of 1060 mL. For all other samples in 2013 and 2014, fluid was pumped using a peristaltic pump from the sampling bags or carboys into evacuated 500 mL Pyrex bottles with air-tight butyl stoppers to a volume of 530 mL. Due to limitations in the amount of fluid able to be collected (4 to 5 L), no biological replicates were conducted. During filling, steps were taken to minimize introduction of oxygen and outgassing of fluid. Prior to filling, ^{13}C-labeled sodium bicarbonate (Cambridge Isotope Laboratories, Tewksbury, MA, USA) for the experimental condition or ^{12}C-labeled sodium bicarbonate (Sigma, St. Louis, MO, USA) for the control condition was added to each bottle to a final concentration of 10 mM over background. After filling, the pH of each bottle was measured using pH paper and then adjusted to vent fluid pH (<6.5) by adding 1–2.5 mL of 10% HCl. The headspace was filled with pure H_2 gas using a syringe in the quantity of 20 mL (1698 μmol/kg) for each 500 mL bottle and 60 mL (2547 μmol/kg) for the 1L bottles. ^{12}C- and ^{13}C-bicarbonate amended bottles were each incubated at 30, 55, and 80°C for various times as shown in Table 2 in the main text. After incubation, the fluid in each bottle was filtered through 0.22 μm Sterivex filters (Millipore). Filtration was completed in less than 30 min, and Sterivex filters were immediately preserved in RNALater (Ambion) and frozen at −80°C.

716 RNA from SIP experiments was extracted according to (8) and detailed in the
717 Supplementary Methods. Following RNA extraction and quantification, each RNA-SIP
718 experiment required isopycnic centrifugation to separate the heavy RNA (labeled with ^{13}C—the
719 active autotrophs) from the light RNA (members of the community that did not take up the ^{13}C
720 label, representing the less active members of that community) as described in (8) and the
721 Supplementary Methods.

722 Four metatranscriptomic libraries were constructed for each RNA-SIP experiment: two
723 from the ^{12}C-control (^{12}C-light and ^{12}C-heavy) and two from the ^{13}C-experiment, (^{13}C-light and
724 ^{13}C-heavy) as described in (8) except for four samples: the second timepoints in 2014 of Marker
725 113 at 55°C, Marker 33 at 30°C and 80°C, and the only timepoint at Anemone at 80°C. The ^{12}C-
726 control incubation peak(s) of highest RNA concentration were used to construct the ^{12}C-light
727 library, which represents the natural community. Similarly, the ^{13}C-experiment incubation peak(s)
728 of highest RNA concentration were used to construct the ^{13}C-heavy library, which represents the
729 labeled, active autotrophic community. The other two libraries from each temperature, ^{12}C-heavy
730 and ^{13}C-light, were constructed to act as additional controls but were not taken through full
731 bioinformatic processing. In some cases (denoted in Figs S3-S5), two RNA fractions were
732 combined for library construction.

733 *Metagenomic bioinformatic analyses*

734 All metagenomic libraries were constructed as described in the Supplementary Methods.
735 There were 11 metagenome samples processed, including metagenomes from all three vent sites
736 in 2015 (Table S3; 10). These samples were included to provide a comprehensive functional
737 repertoire in diffuse fluid communities at Axial Seamount (10). A pipeline with code used in
738 metagenomic processing can be found here: https://github.com/corporeal-snow-albatross-

739 5/Axial_Metagenomics. Samples were first trimmed of Illumina adapter sequences using
740 Trimmomatic (v0.32; 55), quality controlled using FastQC (v0.11.9; 56), and quality results were
741 aggregated across samples into a single report using MultiQC (v1.12; 57). These initial trimming
742 and quality control steps were done using the qc-trim Snakemake pipeline
743 (https://github.com/shu251/qc-trim). The separate forward reads and separate reverse reads were
744 combined using the cat (concatenate) command in Unix, and then concatenated forward and
745 reverse read files were combined using the fq2fa (v1.1.3) function within the IDBA_UD assembler
746 (58; https://github.com/loneknightpy/idba). Each of the metagenomes were assembled using
747 IDBA_UD (v1.1.3), using a max kmer size of 120 (58; https://github.com/loneknightpy/idba).
748 Contig and scaffold quality was evaluated using MetaQUAST (v5.0.2; 59), and the best assembly
749 given steps of 20 from kmer lengths of 20-120 was chosen for further analysis. Each metagenome
750 was submitted to the DOE Joint Genome Institute's Integrated Microbial Genome Expert Review
751 (IMG/ER) for annotation. IMG/ER JGI GOLD Analysis Project ID numbers can be found in Table
752 S3. Open reading frame (ORF) information from the IMG/ER annotation was extracted using a
753 python script to create .ffn files from .gff (containing contig and locus identity, start and stop sites
754 of ORFs, and strand information) and .fna files (containing the nucleotide sequence of each ORF).
755 All metagenome .ffn files were then concatenated to make one long, annotated assembly using the
756 cat command in Unix.

757 The ORFs predicted in each metatranscriptomic (mRNA) file were mapped back to the
758 concatenated metagenomic assembly, which was first indexed using the kallisto index function
759 within the pseudoaligner Kallisto prior to mapping (v.0.46.0; 60). Post-mapping, the KEGG
760 Ontology (KO) ID's and the taxonomy of each predicted ORF in the metagenomes were retrieved
761 from IMG/ER. Cutoffs on the minimum requirements of an e-score of 10^{-10}, 30% amino acid

762 identity, and alignment length of 40 amino acids were imposed, as used in (10). Additionally,
763 eukaryote and virus hits were filtered out of the taxonomy file. Before filtering, there were
764 5,432,185 contigs classified as eukaryotes or viruses, and after filtering, the classified contig count
765 was 5,309,746. As a percentage of the classified contigs in the concatenated metagenomic
766 assembly, this results in 2.25% of the total, meaning most hits belonged to prokaryotes. The filtered
767 KO tables of each metagenome were concatenated with each other, and the same was done for the
768 taxonomy tables. The concatenated KO and taxonomy tables were then combined with each other
769 using an inner_join in the R dplyr package (61, 62), based on target_id (predicted ORF).

770 *Metagenome Assembled Genome (MAG) generation and analysis*

771 In addition to an annotated, concatenated assembly, a co-assembly using the quality-
772 filtered and trimmed reads from 11 metagenomic samples was also constructed using MEGAHIT
773 (v1.2.9; 63) with parameters --min-contig-len = 200, --presets = "meta-sensitive". Assembly
774 statistics were checked using MetaQUAST (v5.0.2; 59). The resulting assembly had 2,318,625
775 contigs that were at least 500 bp in length; of those contigs, the N50 = 721 bp and maximum length
776 = 280,659 bp. The co-assembled metagenome (hereafter referred to as the "co-assembly") was
777 annotated through the DOE Joint Genome Institute's Integrated Microbial Genome Expert Review
778 (IMG/ER) pipeline. IMG/ER JGI GOLD Analysis Project ID numbers can be found in Table S3.
779 The resulting gene calls, .gff annotation file, and phylodist taxonomy of contigs, were used as the
780 reference material for the metagenome assembled genomes (MAGs), differential gene expression
781 analyses, taxonomy assessments, and overviews of functional potential versus expression. KEGG
782 Ontology (KO) ID's and the taxonomy of each predicted ORF in the co-assembly were retrieved
783 from IMG/ER. Cutoffs on the minimum requirements of an e-score of 10^{-10}, 30% amino acid
784 identity, and alignment length of 40 amino acids were imposed, as used in (10).

785 MetaBAT2 (v2.15; 64) was used to generate metagenome-assembled genomes (MAGs).
786 The co-assembly was first indexed using the bwa index within BWA mem (v7.17; 65) and then
787 metagenomes were mapped to the indexed file. The resulting output was processed through
788 Samtools (v1.13; 66). The .sam file generated from mapping was converted to a .bam file using the
789 samtools view function and resulting .bam files were sorted using samtools sort. Prior to binning,
790 depth (also called coverage) files were created for each metagenome and binned with a minimum
791 contig length of 1500 using MetaBAT2. DAS Tool was then used to resolve redundancy among
792 bins and provide an optimized bin set (v1.1.7, 67). Bins were taxonomically classified using
793 GTDB-tk (v2.1.1; 68).

794 Genomic binning from all the diffuse fluid metagenomes resulted in 391 MAGs, and after
795 removing redundant bins using DAS Tool (v1.1.7; 67), 120 bins remained with 45 having < 10%
796 contamination and being >70% complete (Table S5). The MAGs were further filtered to remove
797 heterotrophs and samples solely sourced from the plume, background, or 2015 metagenomes,
798 resulting in 25 bins remaining. The final 11 MAGs were selected based on having >4% of their
799 coding genome expressed (length of expressed genes (bp)/genome length (bp); Fig 4 in the main
800 text, Table S6) in any individual RNA-SIP ^{13}C-enriched metatranscriptome fraction.

801 *Metatranscriptomic bioinformatic analyses*

802 Metatranscriptomic libraries from unmanipulated fluids were constructed as described in the
803 Supplementary Methods. In total, there were 84 metatranscriptome samples processed: 6
804 metatranscriptomes from unmanipulated fluids at each vent in 2013 and 2014 and 78 RNA-SIP
805 metatranscriptomes (Tables S3). A pipeline containing the code used to process
806 metatranscriptomes is located here: https://github.com/corporeal-snow-albatross-
807 5/Axial_Metatranscriptome. Metatranscriptomic sequences were trimmed and quality checked

808 with the same methods and software parameters as the metagenomic sequences. The separate
809 forward reads and separate reverse reads were concatenated using the cat command in Unix, and
810 then concatenated forward and reverse read files were combined using Fast Length Adjustment of
811 Short reads (FLASH; v.1.2.11; 69), which is a program used to combine fastq files. The only
812 parameter set was for read length, which was 110 bp. Although metatranscriptome libraries were
813 constructed with selective amplification for mRNA (not rRNA), the SIP metatranscriptomes were
814 not. To separate the rRNA for preliminary taxonomic analyses from the mRNA for downstream
815 processing, SortMeRNA (v4.2.0; 70) was used (Table S4). The SILVA v.132 bacterial and
816 archaeal 16S (id85), 23S (id98), and 5S (id98) databases were used as reference databases to map
817 the rRNA. The rest of the parameters were: --fastx for a fastq output format, --other for mRNA
818 reads that did not map to the databases, --out2, and --pairedout for non-aligned reads. The
819 percentage of reads mapping to rRNA from SortMeRNA can be found in Table S4.

820 Fastq reads from SortMeRNA rRNA output were converted to fasta format using the fq2fa
821 (v.1.1.3) function within IDBA_UD assembler (58; https://github.com/loneknightpy/idba). rRNA
822 taxonomy was classified using mothur classify.seqs function and the SILVA (v.132) 16S rRNA
823 reference database (71). The 5S rRNA database used as one of the reference databases for rRNA
824 mapping in SortMeRNA also contains eukaryotes. As such, the eukaryote hits were removed
825 before further processing. Taxonomy count tables were generated using R (61), and bar plotting
826 for rRNA was done via ggplot2 (72) within tidyverse (73) in R. Resulting plots were only used to
827 compare to ORF transcript taxonomy and are not included in this paper.

828 Fastq mRNA reads were mapped to the indexed concatenated metagenomic assembly using
829 the kallisto quant function within Kallisto (v0.46.0; 60), which also normalized all ORFs that
830 mapped, providing transcripts per million (tpm) values for each ORF. Sample names were attached

831 to kallisto output files, then all files were concatenated and tpm values of 0 were removed. This
832 table was then attached to the KO and taxonomy table made from the IMG/ER output using an
833 inner_join in the R dplyr package (61, 62), based on target_id (predicted ORF). 784,486 total ORFs
834 from all samples joined out of 4,027,381 total, which means that 80.521% of ORFs from the
835 concatenated metagenome were unmatched in KO and taxonomy in the metatranscriptomes and
836 SIP metatranscriptomes. There were no eukaryote hits in the ORFs that had a match with both KO
837 and taxonomy. There were only 11 virus hits in these samples of 784,486 total ORFs that did have
838 matching KO's and taxonomy. Because few viruses and no eukaryotes were found, they were
839 removed for further processing and to enable comparability between the rRNA and ORF taxonomy.
840 All figures and statistical analyses were completed in R (61).

841 *Differential expression analysis*

842 Metatranscriptomic (mRNA) samples from the ^{13}C-enriched fractions of Marker 113,
843 Anemone, and Marker 33 incubations at 30, 55, and 80°C from 2013 and 2014 were pseudoaligned
844 to the indexed co-assembly using kallisto (parameters: --single -l 151 -s 41) (v0.46.0; 60). The
845 kallisto outputs of metatranscriptome pseudocounts were tabulated with the R package tximport
846 (v1.26.1; 36) using a custom annotation database of unique genes collapsed into protein-coding
847 gene representatives. Due to the diversity in metagenomes, the co-assembly annotation contained
848 multiple targets for gene products. To reduce complexity in functional expression analyses,
849 protein-coding genes observed in the co-assembly were indexed into protein families using IMG's
850 highest confidence annotation such as KEGG, COG, pfam, and TIGRFAM. ORFs annotated with
851 only "hypothetical protein" were discarded. The annotation database indexed 2,428,812 genes
852 representing 14,942 unique genes collapsed into protein-coding gene representatives observed in

853 the co-assembly. When referring to genes and proteins in our evaluations of differential functional
854 expression, we are using this consolidated database.

855 Differential expression analyses were conducted in R with DESeq2 (v1.38.3; 34, 35), and
856 code can be found here: https://github.com/corporeal-snow-albatross-
857 5/Axial_Differential_Expression. 3Our experimental design included three different conditions
858 (vent, temperature, and year) with two or more levels (the possible values each variable can take
859 in the DE statistical model). For vent, there are three levels: Marker 113, Anemone, and Marker
860 33; for temperature there are also three levels: 30°C, 55°C, and 80°C; for year, there are two levels:
861 2013 and 2014. Because the number of samples across conditions was uneven (i.e. the number of
862 RNA-SIP experiments differed between years and across vents and temperatures, Table 2), we
863 implemented methodology for imbalanced designs and multi-group data, as described in Love *et*
864 *al*., 2014b (35). First, we manually defined contrasts (grouping of samples for each comparison)
865 to account for an imbalance of samples in the DESeq2 model design (37, 38). This allowed for the
866 model to identify differential gene expression without requiring an untreated control. Subsetting
867 the dataset minimized the observed within-group variability caused by unparameterized interaction
868 of variables, thereby reducing stochasticity and improving assessment of significant genes. This
869 permitted us to tailor baseline gene expression for each of the three comparisons: across
870 experimental temperatures within each vent (1030 significantly differentially expressed (SDE)
871 transcripts; Table S10), across vents by temperature (329 SDE transcripts; Table S11), and
872 between 2013 and 2014 within each vent (161 SDE transcripts; Table S12).

873 For temperature comparisons within each vent (i.e. all Anemone experiments at 30, 55, and
874 80°C compared to one another), the baseline expression for genes was the normalized expression
875 of all ^{13}C-enriched metatranscriptomic fractions (n=21; Table 2). For across vent comparisons at

876 a single temperature (i.e. All 30°C experiments across all vents), as well as comparisons between
877 years within each vent (i.e. 2013 Marker 113 80°C incubation compared to 2014 Marker 113 80°C
878 incubation), gene baseline expressions were calculated at each incubation temperature: 6 ^{13}C-
879 enriched metatranscriptomes at 30°C; 8 ^{13}C-enriched metatranscriptomes at 55°C; and 7 ^{13}C-
880 enriched metatranscriptomes at 80°C. Volcano plots show genes with p-values adjusted for
881 multiple test correction using the Benjamini-Hochberg procedure to control the false discovery
882 rate (FDR, 35), with padj < 0.001 and log2 fold-change > |2|; only genes involved in carbon
883 fixation, hydrogen, methane, nitrogen, oxygen, and sulfur metabolism are shown in Figures 6,
884 S10A-C, and S11A-C. Plots with expanded gene function annotations are shown in Figures S9,
885 S10D-F, and S11D-F. For additional details about how the differential expression analysis was
886 conducted, see the Supplementary Methods.

887 **DATA AVAILABILITY**

888 All raw metagenomic and metatranscriptomic read data are publicly available through the
889 Sequence Read Archive (SRA). Metagenomic assemblies are publicly available through JGI
890 GOLD. All accession numbers are located in Table S3.

891 **ACKNOWLEDGEMENTS**

892 This work was funded by the Gordon and Betty Moore Foundation Grant GBMF3297; the
893 NSF Center for Dark Energy Biosphere Investigations (C-DEBI) (OCE-0939564), contribution
894 number TBD, NOAA/PMEL, contribution number TBD; the Joint Institute for the Study of the
895 Atmosphere and Ocean (JISAO) under NOAA Cooperative Agreement NA15OAR4320063,
896 contribution number TBD; and the National Aeronautics and Space Administration (NASA) grant
897 number 80NSSC19K1427.

The NOAA/PMEL supported this work with ship time in 2014 and through funding to the Earth Ocean Interactions group. The 2013 data collected in this study includes work supported by the Schmidt Ocean Institute during cruise FK010–2013 aboard R/V Falkor. The NOAA/PMEL (through funding to the Earth Ocean Interactions group) and GBMF supported field work in 2014 with ship and vehicle time aboard the R/V Brown (RB2014-03). We thank the captains and crews of the *R/V Falkor, R/V Thompson* and *R/V Brown* as well as the outstanding ROV teams of the vehicles *ROPOS*, *SuBastian*, and *JASON*.

Sarah Hu, Connor Scannerton, and Margrethe Serres provided guidance on the analysis and code used to process this dataset, while the Keck Facility at the Josephine Bay Paul Center at the Marine Biological Laboratory provided support for sequencing. Kevin Roe, Noah Lawrence-Slavas, Susan Merle, Andra Bobbit, and William Chadwick provided support at sea.

SUPPLEMENTARY INFORMATION

<u>Tables:</u>

1. **Table S1**: Chemistry
2. **Table S2**: Oxygen data
3. **Table S3:** metatranscriptome and RNA-SIP metatranscriptome samples with accession numbers
4. **Table S4**: SortMeRNA results: percent rRNA in the metatranscriptome samples
5. **Table S5:** MAG statistics for high completeness, low contamination bins (120 total)
6. **Table S6:** Input data to the MAGs
7. **Table S7:** Input data to the bubble plots
8. **Table S8:** Functions represented in the bubble plot matched with the taxa doing them
9. **Table S9**: Table with number of SDE genes by condition

921 10. **Table S10:** Across temperatures within each vent, DE analysis

922 11. **Table S11:** Across vents at each experimental temperature, DE analysis

923 12. **Table S12:** From 2013 to 2014 at each vent, DE analysis

924 13. **Table S13:** Hydrogenases in the community functional analysis and bins

925 **Figures:**

926 1. **Figure S1**: Map of Axial

927 2. **Figure S2**: Cl^- vs Mg

928 3. **Figure S3**: qPCR at 30°C

929 4. **Figure S4:** qPCR at 55°C

930 5. **Figure S5:** qPCR at 80°C

931 6. **Figure S6:** non-rRNA taxonomy bar plots with both 12L and 13H fraction taxonomy shown

932 7. **Figure S7:** Phylogenetic tree of 120 quality-filtered MAGs

933 8. **Figure S8:** Top 30 TPM at each temperature

934 9. **Figure S9:** Volcano plot with expanded genes annotated by general functional category

935 showing differential expression across experimental temperature within each vent

936 10. **Figure S10:** Volcano plot showing differential expression of genes across vents by

937 experimental temperature, with the top panel showing a limited gene set matching those in

938 Fig 5, and the bottom panel with expanded gene annotation by general functional category

939 11. **Figure S11**: Volcano plot showing differential expression of genes between 2013 and 2014

940 within each vent, with the top panel showing a limited gene set matching those in Fig 5, and

941 the bottom panel with expanded gene annotation by general functional category

942 12. **Figure S12:** Presence/absence plot of transcribed electron acceptors by *Sulfurimonas* vs

943 *Hydrogenimonas* in 30 and 55°C RNA-SIP experiments.

944 **SUPPLEMENTARY METHODS**

945 **RNA Extraction from Sterivex filter**

946 RNA from SIP experiments was extracted according to (8) by first cutting the Sterivex
947 filter into pieces with a sterile razor blade then following the protocol in the mirVana miRNA
948 isolation kit (Ambion). Biological material was removed from the filter pieces with a bead-beating
949 step using RNA PowerSoil beads (MoBio, Carlsbad, CA, USA), followed by an extraction with
950 acid phenol:chloroform. A total volume of 100 µL RNA was extracted and any remaining DNA
951 was removed using the Turbo-DNase kit (Ambion).

952 **Isopycnic centrifugation, fractionation and qRT-PCR**

953 Following RNA extraction and quantification, each RNA-SIP experiment required
954 isopycnic centrifugation to separate the heavy RNA (labeled with ^{13}C—the active autotrophs) from
955 the light RNA (members of the community that did not take up the ^{13}C label, representing the less
956 active members of the community) as described in (8). To prepare the gradient solution for each
957 sample, 5.1 mL of CsTFA (~2 g mL-1; GE Healthcare Life Sciences, Piscataway, NJ, USA), 185
958 µL formamide, and a mixture of 500-750 ng RNA and gradient buffer solution (0.1 M Tris-HCl,
959 0.1 M KCl, 0.1 mM EDTA) up to 1 mL were first mixed in a 15 mL falcon tube prior to
960 centrifugation (25). Once mixed, the refractive index was measured for each sample to ensure a
961 median RI of 1.3729 +/- 0.0002, equating to a density of ~ 1.80 g mL-1. Samples were then loaded
962 into 4.9 mL OptiSeal tubes (Beckman Coulter, Brea, CA, USA), weighed to ensure proper balance,
963 placed into a VTi 65.2 vertical rotor (Beckman Coulter), and spun at 37,000 r.p.m. at 20°C for 64
964 hr using an Optima L-80 XP ultracentrifuge (Beckman Coulter). Each gradient was fractionated
965 into 12 tubes of approximately 410 µL each. The refractive index of each fraction was measured
966 to determine density as described in Lueders, 2010 (25; Equation 1). RNA was precipitated with

967 ice-cold isopropanol and the pellet was washed with ice-cold 70% ethanol as also described in
968 (25). Following centrifugation, the RNA concentration of each fraction was determined using the
969 RiboGreen quantification kit (Invitrogen) and a Gemini XPS plate reader (Molecular Devices,
970 Sunnyvale, CA, USA). The RNA concentration was used as the guide for selecting which fractions
971 to sequence. Quantitative reverse transcription polymerase chain reaction (qRT-PCR) was used to
972 determine the quantity (copy number) of the 16S rRNA gene within each fraction using the KAPA
973 Biosystems SYBR FAST One Step RT-qPCR (ABI Prism) and the Universal 16S rRNA primers,
974 Pro341F and Pro805R primers (74). E. coli ribosomal RNA was used to construct a standard curve.
975 Results were used to determine the ratio of maximum quantity of 16S rRNA within each set of
976 fractions, that is the ratio of 16S rRNA in each fraction to the maximum copy number across all
977 fractions (25, 29, 30; Figs S3-S5).

978 **Equation 1.** Lueders equation for fraction density (CsTFA + Gradient Buffer + Formamide)

979 $$y = -1893.9820x^2 + 5230.8018x - 3609.6804$$

980 **Metagenomic and Metatranscriptomic Library Construction**

981 Library construction for RNA-SIP fractions was carried out as described in Fortunato and
982 Huber (2016) (8). Briefly, double stranded cDNA was constructed using SuperScript III First-
983 strand synthesis system (Invitrogen, Grand Island, NY, USA) and mRNA second strand synthesis
984 module (NEB, Ipswich, MA, USA). The synthesized double stranded cDNA was sheared to a
985 fragment size of 175 bp using a Covaris S-series sonicator (Woburn, MA, USA). SIP
986 metatranscriptomic library construction was completed using the Ovation Ultralow Library
987 Complete Prokaryotic RNA-Seq DR multiplex system (Nugen, San Carlos, CA, USA) following
988 manufacturer instructions, amplified using 15 cycles. Ribosomal RNA was not removed before
989 the construction of libraries. Sequencing was performed on an Illumina HiSeq 1000 at the W.M.

990 Keck sequencing facility at the Marine Biological Laboratory in Woods Hole, MA. All libraries
991 were paired-end, with a 30 bp overlap, resulting in an average merged read length of 110 bp.
992 The 47 mm flat filters that were collected and preserved in situ for metagenomic and
993 metatranscriptomic sequencing were processed according to (10). The filters were first cut in half
994 with a sterile razor; half used for DNA extraction for metagenomic sequencing, and half used for
995 RNA extraction for metatranscriptome sequencing. For DNA extraction, the DNA filter was rinsed
996 with sterile PBS to remove the salts from the RNALater and was then extracted using a phenol-
997 chloroform method adapted from (75) and (76). DNA was then sheared to a fragment size of 175
998 bp (2013 and 2014) or 275 bp (Anemone, Marker 33, Marker 113 metagenomes from 2015, plume,
999 and background seawater) using a Covaris S-series sonicator. Metagenomic library construction
1000 was completed using the Ovation Ultralow Library DR multiplex system (Nugen) following
1001 manufacturer instructions. RNA was extracted using the mirVana miRNA isolation kit (Ambion).
1002 Ribosomal RNA removal, cDNA synthesis, and metatranscriptomic library preparation was
1003 carried out using the Ovation Complete Prokaryotic RNA-Seq DR multiplex system (Nugen)
1004 following manufacturer instructions.

1005 **Metagenomic and Metatranscriptomic Sequencing**

1006 Metagenomic and metatranscriptomic sequencing was done on an Illumina HiSeq 1000 in
1007 2013 and 2014 and an Illuma NextSeq 500 in 2015. All libraries were paired-end, with a 30 bp
1008 overlap, resulting in an average merged read length of 110 bp for libraries from 2013 and 2014
1009 and 151 bp for libraries from 2015. Metagenomic and metatranscriptomic sequencing was carried
1010 out at the W.M. Keck sequencing facility at the Marine Biological Laboratory in Woods Hole,
1011 Massachusetts.
1012

1013 **Differential Expression Analysis**

1014 *Defining contrasts for differential expression*

1015 DESeq2 statistically compares abundances of genes across experimental conditions (34).
1016 A common implementation of DESeq2 is for the quantitative analysis of RNA-seq data to test the
1017 null hypothesis that gene expression is unchanged between two groups (34, 35, 37). However,
1018 DESeq2 can also robustly interpret experimental designs with multiple variables and/or high
1019 within-group variability in gene expression and imbalanced sample replication. In this study, we
1020 examined how temperature, time, and/or the vent's unique chemistry affect expression patterns
1021 and metabolisms of chemoautotrophs. Since all of the data examined for differential expression
1022 are from ^{13}C-incubated samples, it would be erroneous to consider the unmanipulated fluids as the
1023 control for each of these models because that does not allow us to disentangle the interaction of
1024 ^{13}C-isotope spike + incubation temperature + incubation time as an influence on the expression
1025 profiles. We customized our input and models to reduce stochasticity in gene dispersion estimates,
1026 accommodate the three conditions (vent, temperature, and year) with multiple levels, and address
1027 specific hypotheses about chemoautotrophy in these vents.

1028 For example, to explore differential gene expression in chemoautotrophs at 80°C due to
1029 vent chemistry (i.e. between Marker 113, Marker 33, and Anemone), we subset the data to reduce
1030 variability in modeled gene dispersion estimates as a result of temperature (i.e. remove the 30°C
1031 and 55°C profiles), and remove the interaction effect of time by considering as replicates the vent-
1032 specific samples across different years incubated at 80°C. In this examination, the baseline
1033 'expected' gene expression profile is calculated from the ^{13}C-enriched samples incubated at 80˚C
1034 (n=7).

1035 When determining differential expression due to incubation temperature in each vent, we
1036 still aimed to be able to compare these results between vents. To enable these comparisons, we
1037 used all 21 of the ^{13}C-enriched samples to estimate gene baseline expression. Then in the model,
1038 we removed year as a variable, subset the dataset by vent, and allowed for temperature to vary.
1039 These contrasts can then be built for each comparison of interest as described in the main
1040 manuscript and Methods (37).

1041 *Sample "replicates"*

1042 For the vent-specific across-temperature comparisons, we considered timepoints and
1043 different years as 'replicates' (collapsing ^{13}C-enriched metatranscriptomes by time). For the
1044 across-vents, temperature-specific comparisons, we collapsed ^{13}C-enriched metatranscriptomes by
1045 time again. For the within-vent, within-temperature, across years comparison, we considered
1046 timepoints of ^{13}C-enriched metatranscriptomes as replicates.

1047 *Choice of baseline*

1048 As noted, a baseline of the unmanipulated metatranscriptomic expression was not used,
1049 because it would not accurately capture comparisons of an isotope-spiked sample across
1050 temperature and between years. Instead, a baseline (grouped by specific comparison) of averaged
1051 ^{13}C-enriched transcript abundance for each condition was chosen (13H only), instead of an average
1052 of ^{12}C-light control transcripts + ^{13}C-enriched transcripts (13H + 12L) or the average of only ^{12}C-
1053 light transcripts (12L only) from the RNA-SIP experiments. These normalized expression analyses
1054 support the determination to use only ^{13}C-enriched samples in our DE contrasts, since the patterns
1055 (number of SDE genes and in which direction) in each comparison are not substantially changed
1056 when we choose a different contrast (13H vs 13H + 12L), and 13H contrasts produced a slightly
1057 higher number of SDE genes than the 13H + 12L baseline.

1058 **REFERENCES**

1059 1. Dick GJ. 2019. The microbiomes of deep-sea hydrothermal vents: distributed globally, shaped
1060 locally. *Nat Rev Microbiol* 17:271–283.
1061 2. Jannasch HW, Mottl MJ. 1985. Geomicrobiology of deep-sea hydrothermal vents. *Science*
1062 229:717–725.
1063 3. Summit M, Baross JA. 2001. A novel microbial habitat in the mid-ocean ridge subseafloor.
1064 *Proc Natl Acad Sci* 98:2158–2163.
1065 4. Reysenbach A-L, Shock E. 2002. Merging genomes with geochemistry in hydrothermal
1066 ecosystems. *Science* 296:1077–1082.
1067 5. McCollom TM. 2005. Energetic constraints on subsurface biomass production within the
1068 igneous ocean crust. *Geochimica et Cosmochimica Acta* 69:A200.
1069 6. Huber JA, Holden JF. 2008. Modeling the impact of diffuse vent microorganisms along mid-
1070 ocean ridges and flanks. *In* Magma to Microbe: Modeling Hydrothermal Processes at Ocean
1071 Spreading centers Jan 1;178:215-31.
1072 7. Amend JP, McCollom TM, Hentscher M, Bach W. 2011. Catabolic and anabolic energy for
1073 chemolithoautotrophs in deep-sea hydrothermal systems hosted in different rock types.
1074 *Geochim Cosmochim Acta* 75:5736–5748.
1075 8. Fortunato CS, Huber JA. 2016. Coupled RNA-SIP and metatranscriptomics of active
1076 chemolithoautotrophic communities at a deep-sea hydrothermal vent. *ISME J* 10:1925–1938.
1077 9. Olins HC, Rogers DR, Preston C, Ussler W 3rd, Pargett D, Jensen S, Roman B, Birch JM,
1078 Scholin CA, Haroon MF, Girguis PR. 2017. Co-registered Geochemistry and
1079 Metatranscriptomics Reveal Unexpected Distributions of Microbial Activity within a
1080 Hydrothermal Vent Field. *Front Microbiol* 8:1042.

10. Fortunato CS, Larson B, Butterfield DA, Huber JA. 2018. Spatially distinct, temporally stable microbial populations mediate biogeochemical cycling at and below the seafloor in hydrothermal vent fluids. *Environ Microbiol* 20:769–784.

11. McNichol J, Stryhanyuk H, Sylva SP, Thomas F, Musat N, Seewald JS, Sievert SM. 2018. Primary productivity below the seafloor at deep-sea hot springs. *Proc Natl Acad Sci* 115:6756–6761.

12. Opatkiewicz AD, Butterfield DA, Baross JA. 2009. Individual hydrothermal vents at Axial Seamount harbor distinct subseafloor microbial communities. *FEMS Microbiol Ecol* 70:413–424.

13. Perner M, Bach W, Hentscher M, Koschinsky A, Garbe-Schönberg D, Streit WR, Strauss H. 2009. Short-term microbial and physico-chemical variability in low-temperature hydrothermal fluids near 5 degrees S on the Mid-Atlantic Ridge. *Environ Microbiol* 11:2526–2541.

14. Perner M, Hansen M, Seifert R, Strauss H, Koschinsky A, Petersen S. 2013. Linking geology, fluid chemistry, and microbial activity of basalt- and ultramafic-hosted deep-sea hydrothermal vent environments. *Geobiology* 11:340–355.

15. Huber JA, Mark Welch DB, Morrison HG, Huse SM, Neal PR, Butterfield DA, Sogin ML. 2007. Microbial population structures in the deep marine biosphere. *Science* 318:97–100.

16. Huber JA, Cantin HV, Huse SM, Welch DBM, Sogin ML, Butterfield DA. 2010. Isolated communities of Epsilonproteobacteria in hydrothermal vent fluids of the Mariana Arc seamounts. *FEMS Microbiol Ecol* 73:538–549.

17. Akerman NH, Butterfield DA, Huber JA. 2013. Phylogenetic diversity and functional gene patterns of sulfur-oxidizing subseafloor Epsilonproteobacteria in diffuse hydrothermal vent fluids. *Front Microbiol* 4:185.

18. Larson BI, Houghton JL, Lowell RP, Farough A, Meile CD. 2015. Subsurface conditions in hydrothermal vents inferred from diffuse flow composition, and models of reaction and transport. *Earth Planet Sci Lett* 424:245–255.

19. Meier D. 2016. PhD Thesis. University of Bremen, Bremen, Germany. Bacterial niche adaptation at hydrothermal vents.

20. Reveillaud J, Reddington E, McDermott J, Algar C, Meyer JL, Sylva S, Seewald J, German CR, Huber JA. 2016. Subseafloor microbial communities in hydrogen-rich vent fluids from hydrothermal systems along the Mid-Cayman Rise. *Environ Microbiol* 18:1970–1987.

21. Galambos D, Anderson RE, Reveillaud J, Huber JA. 2019. Genome-resolved metagenomics and metatranscriptomics reveal niche differentiation in functionally redundant microbial communities at deep-sea hydrothermal vents. *Environ Microbiol* 21:4395–4410.

22. Fullerton H, Smith L, Enriquez A, Butterfield D, Wheat CG, Moyer CL. 2024. Seafloor incubation experiments at deep-sea hydrothermal vents reveal distinct biogeographic signatures of autotrophic communities. *FEMS Microbiol Ecol* 100.

23. Trembath-Reichert E, Butterfield DA, Huber JA. 2019. Active subseafloor microbial communities from Mariana back-arc venting fluids share metabolic strategies across different thermal niches and taxa. *ISME J* 13:2264–2279.

24. Fortunato CS, Butterfield DA, Larson B, Lawrence-Slavas N, Algar CK, Zeigler Allen L, Holden JF, Proskurowski G, Reddington E, Stewart LC, Topçuoğlu BD, Vallino JJ, Huber JA. 2021. Seafloor incubation experiment with deep-sea hydrothermal vent fluid reveals effect of pressure and lag time on autotrophic microbial communities. *Appl Environ Microbiol* 87.

1125 25. Lueders T. 2010. Stable isotope probing of hydrocarbon-degraders. p 4011–4026. In Timmis
1126 KN (ed), Handbook of Hydrocarbon and Lipid Microbiology. Springer, Berlin.
1127 https://doi.org/10.1007/978-3-540-77587-4_312
1128 26. Lueders T, Dumont MG, Bradford L, Manefield M. 2016. RNA-stable isotope probing: from
1129 carbon flow within key microbiota to targeted transcriptomes. *Curr Opin Biotechnol* 41:83–
1130 89.
1131 27. Butterfield DA, Roe KK, Lilley MD, Huber JA, Baross JA, Embley RW, Massoth GJ. 2004.
1132 Mixing, reaction and microbial activity in the sub-seafloor revealed by temporal and spatial
1133 variation in diffuse flow vents at Axial Volcano. *In* The Subseafloor Biosphere at Mid-Ocean
1134 Ridges 144:269–289.
1135 28. Stewart LC, Algar CK, Fortunato CS, Larson BI, Vallino JJ, Huber JA, Butterfield DA, Holden
1136 JF. 2019. Fluid geochemistry, local hydrology, and metabolic activity define methanogen
1137 community size and composition in deep-sea hydrothermal vents. *ISME J* 13:1711–1721.
1138 29. Glaubitz S, Lueders T, Abraham WR, Jost G, Jürgens K, Labrenz M. 2009. 13C-isotope
1139 analyses reveal that chemolithoautotrophic Gamma- and Epsilonproteobacteria feed a
1140 microbial food web in a pelagic redoxcline of the central Baltic Sea. *Environ Microbiol*
1141 11:326–337. https://doi.org/10.1111/j.1462-2920.2008.01772.x
1142 30. Bradford LM, Vestergaard G, Táncsics A, Zhu B, Schloter M, Lueders T. 2018.
1143 Transcriptome-stable isotope probing provides targeted functional and taxonomic insights into
1144 microaerobic pollutant-degrading aquifer microbiota. *Front Microbiol* 9:2696.
1145 https://doi.org/10.3389/fmicb.2018.02696
1146 31. Zhou Z, Tran PQ, Cowley ES, Trembath-Reichert E, Anantharaman K. 2024. Diversity and
1147 ecology of microbial sulfur metabolism. *Nat Rev Microbiol* 23:122–140.

1148 32. Takai K, Campbell BJ, Cary SC, Suzuki M, Oida H, Nunoura T, Hirayama H, Nakagawa S,
1149 Suzuki Y, Inagaki F, Horikoshi K. 2005. Enzymatic and genetic characterization of carbon and
1150 energy metabolisms by deep-sea hydrothermal chemolithoautotrophic isolates of
1151 Epsilonproteobacteria. *Appl Environ Microbiol* 71:7310–7320.
1152 33. Nakagawa S, Takai K. 2008. Deep-sea vent chemoautotrophs: diversity, biochemistry and
1153 ecological significance: Chemoautotrophy in deep-sea vents. *FEMS Microbiol Ecol* 65:1–14.
1154 34. Love MI, Huber W, Anders S. 2014a. Moderated estimation of fold change and dispersion
1155 for RNA-seq data with DESeq2. *Genome Biol* 15:550.
1156 35. Love MI, Anders S, Huber W. 2014b. Differential analysis of count data–the DESeq2
1157 package. *Genome Biol* 15:550. https://doi.org/10.1186/s13059-014-0550-8
1158 36. Soneson C, Love MI, Robinson MD. 2015. Differential analyses for RNA-seq: transcript-
1159 level estimates improve gene-level inferences. F1000Res 4:1521.
1160 https://doi.org/10.12688/f1000research.7563.2
1161 37. Tavares H. 2023. DESeq2 contrasts tutorial. GitHub.
1162 https://github.com/tavareshugo/tutorial_DESeq2_contrasts/blob/main/DESeq2_contrasts.md
1163 (Accessed 20 June 2025).
1164 38. Love MI, Huber W, Anders S. 2025. DESeq2: Differential gene expression analysis based on
1165 the negative binomial distribution. Bioconductor.
1166 https://www.bioconductor.org/packages/devel/bioc/vignettes/DESeq2/inst/doc/DESeq2.html
1167 #expanded-model-matrices (Accessed 20 June 2025).
1168 39. Ver Eecke HC, Butterfield DA, Huber JA, Lilley MD, Olson EJ, Roe KK, Evans LJ, Merkel
1169 AY, Cantin HV, Holden JF. 2012. Hydrogen-limited growth of hyperthermophilic
1170 methanogens at deep-sea hydrothermal vents. *Proc Natl Acad Sci* 109:13674–13679.

1171 40. Nübel T, Klughammer C, Huber R, Hauska G, Schütz M. 2000. Sulfide:quinone
1172 oxidoreductase in membranes of the hyperthermophilic bacterium Aquifex aeolicus (VF5).
1173 *Arch Microbiol* 173:233–244.
1174 41. Takai K, Nealson KH, Horikoshi K. 2004. Hydrogenimonas thermophila gen. nov., sp. nov.,
1175 a novel thermophilic, hydrogen-oxidizing chemolithoautotroph within the epsilon-
1176 Proteobacteria, isolated from a black smoker in a Central Indian Ridge hydrothermal field.
1177 *Int J Syst Evol Microbiol* 54:25–32.
1178 42. Perner M, Hentscher M, Rychlik N, Seifert R, Strauss H, Bach W. 2011. Driving forces behind
1179 the biotope structures in two low-temperature hydrothermal venting sites on thesouthern Mid-
1180 Atlantic Ridge: Driving forces behind vent biotopes. *Environ Microbiol Rep* 3:727–737.
1181 43. Nishimura H, Kitano Y, Inoue T, Nomura K, Sako Y. 2010. Purification and characterization
1182 of membrane-associated hydrogenase from the deep-sea epsilonproteobacterium
1183 Hydrogenimonas thermophila. *Biosci Biotechnol Biochem* 74:1624–1630.
1184 44. Campbell BJ, Smith JL, Hanson TE, Klotz MG, Stein LY, Lee CK, Wu D, Robinson JM,
1185 Khouri HM, Eisen JA, Cary SC. 2009. Adaptations to submarine hydrothermal environments
1186 exemplified by the genome of *Nautilia profundicola. PLoS* Genet 5:e1000362.
1187 45. Kubik BC, Holden JF. 2024. Non-thermodynamic factors affect competition between
1188 thermophilic chemolithoautotrophs from deep-sea hydrothermal vents. *Appl Environ*
1189 *Microbiol* 90:e0029224.
1190 46. Stewart LC. 2015. PhD thesis. University of Massachusetts Amherst, Amherst, MA. Energetic
1191 Limitations of Thermophilic Methanogens And Thiosulfate Reducers in The Subsurface
1192 Biosphere at Deep-Sea Hydrothermal Vents.

1193 47. Stewart LC, Llewellyn JG, Butterfield DA, Lilley MD, Holden JF. 2016. Hydrogen and
1194 thiosulfate limits for growth of a thermophilic, autotrophic Desulfurobacterium species from a
1195 deep-sea hydrothermal vent. *Environ Microbiol Rep* 8:196–200.
1196 48. Kristjansson JK, Schönheit P, Thauer RK. 1982. Different K_s values for hydrogen of
1197 methanogenic bacteria and sulfate reducing bacteria: An explanation for the apparent inhibition
1198 of methanogenesis by sulfate. *Arch Microbiol* 131:278–282.
1199 49. Lovley DR, Dwyer DF, Klug MJ. 1982. Kinetic analysis of competition between sulfate
1200 reducers and methanogens for hydrogen in sediments. *Appl Environ Microbiol* 43:1373–1379.
1201 50. Robinson JA, Tiedje JM. 1984. Competition between sulfate-reducing and methanogenic
1202 bacteria for H_2 under resting and growing conditions. *Arch Microbiol* 137:26–32.
1203 51. Takai K, Nealson KH, Horikoshi K. 2004. Hydrogenimonas thermophila gen. nov., sp. nov., a
1204 novel thermophilic, hydrogen-oxidizing chemolithoautotroph within the epsilon-
1205 Proteobacteria, isolated from a black smoker in a Central Indian Ridge hydrothermal field. *Int*
1206 *J Syst Evol Microbiol* 54:25–32.
1207 52. Campbell BJ, Engel AS, Porter ML, Takai K. 2006. The versatile epsilon-proteobacteria: key
1208 players in sulphidic habitats. *Nat Rev Microbiol* 4:458–468.
1209 53. Sievert SM, Hügler M, Taylor CD, Wirsen CO. 2008. Sulfur oxidation at deep-sea
1210 hydrothermal vents, p. 238–258. *In* Microbial Sulfur Metabolism. Springer Berlin Heidelberg,
1211 Berlin, Heidelberg.
1212 54. Wommack KE, Williamson SJ, Sundbergh A, Helton RR, Glazer BT, Portune K, Craig Cary
1213 S. 2004. An instrument for collecting discrete large-volume water samples suitable for
1214 ecological studies of microorganisms. *Deep Sea Res Part I* 51:1781–1792.

1215 55. Bolger AM, Lohse M, Usadel B. 2014. Trimmomatic: a flexible trimmer for Illumina sequence
1216 data. *Bioinformatics* 30:2114–2120.
1217 56. Lo C-C, Chain PSG. 2014. Rapid evaluation and quality control of next generation
1218 sequencing data with FaQCs. BMC Bioinformatics 15:366.
1219 57. Ewels P, Magnusson M, Lundin S, Käller M. 2016. MultiQC: summarize analysis results for
1220 multiple tools and samples in a single report. *Bioinformatics* 32:3047–3048.
1221 58. Peng Y, Leung HCM, Yiu SM, Chin FYL. 2012. IDBA-UD: a de novo assembler for single-
1222 cell and metagenomic sequencing data with highly uneven depth. *Bioinformatic*s 28:1420–
1223 1428.
1224 59. Mikheenko A, Saveliev V, Gurevich A. 2016. MetaQUAST: evaluation of metagenome
1225 assemblies. *Bioinformatics* 32:1088–1090.
1226 60. Bray NL, Pimentel H, Melsted P, Pachter L. 2016. Near-optimal probabilistic RNA-seq
1227 quantification. *Nat Biotechno*l 34:888.
1228 61. R Core Team. 2021. *R: A language and environment for statistical computing*. R Foundation
1229 for Statistical Computing, Vienna, Austria.
1230 62. Wickham H, François R, Henry L, Müller K. 2023. *dplyr: A grammar of data manipulation*.
1231 R package version 1.1.3. https://CRAN.R-project.org/package=dplyr
1232 63. Li D, Liu C-M, Luo R, Sadakane K, Lam T-W. 2015. MEGAHIT: an ultra-fast single-node
1233 solution for large and complex metagenomics assembly via succinct de Bruijn graph.
1234 *Bioinformatics* 31:1674–1676.
1235 64. Kang DD, Li F, Kirton E, Thomas A, Egan R, An H, Wang Z. 2019. MetaBAT 2: an adaptive
1236 binning algorithm for robust and efficient genome reconstruction from metagenome
1237 assemblies. *PeerJ* 7:e7359.

1238 65. Li H. 2013. Aligning sequence reads, clone sequences and assembly contigs with BWA-MEM.
1239 *arXiv*.
1240 66. Li H, Handsaker B, Wysoker A, Fennell T, Ruan J, Homer N, Marth G, Abecasis G, Durbin
1241 R, 1000 Genome Project Data Processing Subgroup. 2009. The Sequence Alignment/Map
1242 format and SAMtools. *Bioinformatics* 25:2078–2079.
1243 67. Sieber CMK, Probst AJ, Sharrar A, Thomas BC, Hess M, Tringe SG, Banfield JF. 2018.
1244 Recovery of genomes from metagenomes via a dereplication, aggregation and scoring strategy.
1245 *Nat Microbio*l 3:836–843.
1246 68. Chaumeil P-A, Mussig AJ, Hugenholtz P, Parks DH. 2022. GTDB-Tk v2: memory friendly
1247 classification with the genome taxonomy database. *Bioinformatics* 38:5315–5316.
1248 69. Magoč T, Salzberg SL. 2011. FLASH: fast length adjustment of short reads to improve genome
1249 assemblies. *Bioinformatics* 27:2957–2963.
1250 70. Kopylova E, Noé L, Touzet H. 2012. SortMeRNA: fast and accurate filtering of ribosomal
1251 RNAs in metatranscriptomic data. *Bioinformatics* 28:3211–3217.
1252 71. Schloss PD, Westcott SL, Ryabin T, Hall JR, Hartmann M, Hollister EB, Lesniewski RA,
1253 Oakley BB, Parks DH, Robinson CJ, Sahl JW, Stres B, Thallinger GG, Van Horn DJ, Weber
1254 CF. 2009. Introducing mothur: open-source, platform-independent, community-supported
1255 software for describing and comparing microbial communities. *Appl Environ Microbiol*
1256 75:7537–7541.
1257 72. Wickham H. 2016. *ggplot2: Elegant Graphics for Data Analysis*. Springer-Verlag, New York,
1258 NY.
1259 73. Wickham H, Averick M, Bryan J, Chang W, D'Agostino McGowan L, François R, Grolemund
1260 G, Hayes A, Henry L, Hester J, Kuhn M, Lin Pedersen T, Miller E, Bache SM, Müller K, Ooms

1261 J, Robinson D, Seidel DP, Spinu V, Takahashi K, Vaughan D, Wilke C, Woo K, Yutani H.
1262 2019. *Welcome to the tidyverse*. J Open Source Softw 4:1686.
1263 https://doi.org/10.21105/joss.01686
1264 74. Takahashi S, Tomita J, Nishioka K, Hisada T, Nishijima M. 2014. Development of a
1265 prokaryotic universal primer for simultaneous analysis of Bacteria and Archaea using next-
1266 generation sequencing. *PLoS One* 9:e105592.
1267 75. Crump BC, Kling GW, Bahr M, Hobbie JE. 2003. Bacterioplankton community shifts in an
1268 arctic lake correlate with seasonal changes in organic matter source. *Appl Environ Microbiol*
1269 69:2253–2268.
1270 76. Zhou J, Bruns MA, Tiedje JM. 1996. DNA recovery from soils of diverse composition. *Appl*
1271 *Environ Microbiol 62*:316–322.